Chapter 6

Adsorption and desorption kinetics of water molecules on Rh(111)

Adsorption and desorption kinetics of water molecules on the Rh(111) surface were investigated using temperature programed desorption (TPD). Water molecules show a coverage dependent sticking probability and initial sticking probability was estimated to be 0.46. In desorption process, water molecules exhibit coexistence of a dilute, gas like phase together with islands of a condensed phase, both being two dimensional. Based on the model proposed by K. J. Kreuzer and S. H. Payne [Surf. Sci. **200**, L433 (1988).], apparent fractional-order TPD spectrum shape can be interpreted as a first-order desorption in the coexisting region, where two-phase has different sticking probabilities. Using threshold-TPD method, coverage dependence of activation energy (E_d) and preexponential factor (ν_d) for desorption were estimated. They showed weak coverage dependence, where E_d and ν_d were decreased from 60 kJ/mol to 51 kJ/mol and from 4.1×10^{17} s^{-1} to 1.3×10^{14} s^{-1} with increasing coverage, respectively.

6.1 Introduction

There have been a number of reports of submonolayer water adsorption and desorption kinetics for metal surfaces, which is particularly important to understand water related catalytic reactions.[1,2] All of reported results indicate that molecular water adsorption on metals is not activated process. One of the most interesting properties of water-metal surface interaction is the high probability with which water can adsorb at most surfaces. Table 6.1 shows reported results for water adsorption probability; initial sticking probability S_0.[3-14] Adsorption temperature ~100 K corresponds roughly to the conditions for optimum cluster formation on most metals, this illustrate the role of surface features in the sticking of water on metal surfaces. If the S_0 is unity and water molecules aggregate to form island, the adsorbing molecules cannot distinguish between a filled site and an empty site because water molecules adsorb/condense on an ice surface with probability of unity.[3] Therefore, a sticking probability, S, is independent of coverage and multilayer can start to form even before the first layer is saturated. However, in the case of low S_0, S should depend on coverage. Thus the reported results for Rh(111) that low S_0 and coverage independent S conflict each other.[4]

As a reverse process of adsorption, desorption kinetics of water molecules have been studied for last decades. The desorption kinetics provide the adsorption energy of water molecules on the surfaces. In the case of molecularly adsorbed water, desorption simply involves breaking the metal-water and/or any other bonds which holds the molecule at surface.

Most of these studies were performed using temperature programed desorption (TPD). On smooth Au,[13] Ag[15] and Cu[16] surfaces, no state is resolved except for the ice feature, reflecting only a very weak interaction with the metal in these cases. A single desorption state is observed on Pt(111)[17], Pd(111)[18],

Ni(111)[19,20], and Rh(111)[4]. Two desorption states are observed for H_2O/Ru(0001) system, which are assigned to molecularly and dissociatively adsorbed states.[21]

In order to derive quantitative information about the strength of the chemisorption bond from TPD data, these reports assumed the kinetics of the desorption process; desorption order and preexponential factor. Based on these assumptions (first-order and preexponential factor of 10^{13} s^{-1}), adsorption energy is estimated to be ~42 kJ/mol on several surfaces.[1,4,20] However, interpretation of the TPD spectra is more complex. The desorption peak is too narrow for first-order desorption kinetics with a typical preexponential factor of 10^{13} s^{-1}; furthermore, first-order kinetics cannot explain a small shift to higher peak temperatures with increasing coverage (see below).

Another approach, which fits the data more successfully, is to assume first-order desorption kinetics, a typical preexponential factor of 10^{13} s^{-1}, and attractive interactions between particles. In the case of Ni(111) this explains both the peak shape and position well. With this model, an adsorption energy of ~42 kJ/mol is obtained. The coverage dependent attractive lateral interaction term (1.4 kJ/mol) is significantly smaller than single hydrogen bond energies in water (~20 kJ/mol).[20]

In the case of Pt(111), Daschbach *et al.*[17] reported that the desorption kinetics for submonolayer water was of a zero-order, where the activation energy (E_d) and the preexponential factor (ν_d) of desorption were estimated to be 54.2±3 kJ/mol and 1.4±3.5 × 10^{16} ML/s, respectively, using TPD and He specular scattering. The zero order desorption is considered as a result of two-dimensional (2D) two phases which coexist as a high-density condensed phase (2D islands) and a low-density 2D gaslike phase.

In any case, coverage dependence of E_d and ν_d has not been reported without assuming the kinetics except for water/Pt(111)[17]. The qualitative similarities of the TPD spectrum for the hexagonal surfaces suggest that the nature of the desorption process may be similar on all of these smooth metal

planes. Here, I studied the adsorption kinetics (sticking probability and its coverage dependence) and desorption kinetics (TPD spectrum shape and desorption kinetic parameters as a function of coverage) of D_2O/Rh(111) in detail using TPD.

6.2 Experimental

The experimental conditions and sample preparation are described in chapter 2. In this experiment, water (D_2O, $H_2{}^{16}O$, $H_2{}^{18}O$) vapor was introduced through a pulse gas dosing system onto the sample surface. All the isotopic waters, $D_2{}^{16}O$ (Aldrich, isotopic purity 99.96 %), $H_2{}^{16}O$ (Milli-Q), $H_2{}^{18}O$ (Isotec, isotopic purity 95.5 %), were degassed through several freeze-pump-thaw cycles prior to exposure.

In this study, the coverage of water molecules is descried by fractional coverage θ. Coverage measurements were performed using TPD; the water coverage was determined by comparing each integrated area of a TPD spectrum with that at the saturation coverage of the first layer which was prepared at 145 K. We define θ=1.0 at the saturation of the high temperature peak at 180 K in TPD (see Fig. 6.2).

6.3 Results and Discussion

6.3.1 Adsorption kinetics

J. J. Zinck and W. H. Weinberg reported that a dependence of coverage on exposure appears approximately linear suggesting a mobile precursor model of adsorption, and the constant sticking probability (S) of 0.58 is estimated for

H_2O/Rh(111).[4] Coverage dependence of S is an important indicator of the adsorption mechanism. Here, I reexamined the coverage uptake experiment with respect to exposure to obtain detailed adsorption kinetics of water/Rh(111) system.

Figure 6.1 shows a fractional coverage of D_2O on Rh(111) as a function of exposure. Water molecules were adsorbed on Rh(111) at 135 K followed by TPD measurement. With increasing exposure, a growth rate of fractional coverage increases at $\theta \leq 1.0$, and fractional coverage grows linearly at $\theta \geq 1.0$. This growth rate is identical to S. Thus, these results indicate that S depends on coverage in submonolayer region. Note that a multilayer desorption peak was observed at 160 K before the first water layer saturates in this experimental condition ($0.8 \leq \theta \leq 1.0$, $T_a = 135$ K).

I analyze the coverage uptake with a following model (Fig. 6.2). Adsorption processes are given in Fig. 6.2(a). In this experimental condition, water molecules cannot desorb from the surface because adsorption temperature of 135 K is below a desorption onset, 140 K, and water multilayer is not formed [see Fig. 6.3(a)]. In addition, I assume that hot water molecules which dissipate part of an adsorption energy into the substrate can not desorb by substrate thermal fluctuation. This assumption may be consistent with the result that S_0 is not depend on the substrate temperature in the case of water/Pt(111).[1,5] Water molecules impinge on the surface with flux J_{in}. When water molecules impinge on the bare surface with flux $J_{in,\ bare}$, they can reflect from the surface with flux J_{ref} or chemisorb as monomer species (J_{int}) followed by 2D island formation ($J_{int,\ ads}$). Thus, chemisorbed monomer species can be interpreted as an intrinsic precursor in order to form the 2D island where I denote the intrinsic precursor as "A". On the other hand, water molecules impinge on the 2D island with flux $J_{in,\ island}$, they adsorb as an extrinsic precursor with flux J_{ext} on the island and then incorporate into the 2D island ($J_{ext,\ ads}$) where I denote the extrinsic precursor state as "B". Note that we assume that water molecules

cannot reflect from 2D islands like the ice surface as mentioned above. Here, we denote transition probabilities for each process as α, which is schematically illustrated in Fig. 6.2(a) and (b). Using these notation, apparent sticking probability is formulated as

$$\begin{aligned} S(\theta) &= \frac{J_{ads}}{J_{in}} \\ &= \frac{J_{in,bare}}{J_{in}}\alpha_A\alpha_{A,C} + \frac{J_{in,island}}{J_{in}}\alpha_B\alpha_{B,C} \\ &= \frac{J_{in,bare}}{J_{in}}\cdot\frac{J_{int}}{J_{in,bare}}\cdot\frac{J_{int,ads}}{J_{int}} + \frac{J_{in,island}}{J_{in}}\cdot\frac{J_{ext}}{J_{in,island}}\cdot\frac{J_{ext,ads}}{J_{ext}} \\ &= (1-\theta)\cdot\frac{J_{int}}{J_{in,bare}} + \theta \end{aligned} \tag{6.1}$$

where $J_{ads} = J_{int,\,ads} + J_{ext,\,ads}$. Therefore, apparent initial sticking probability, $S(\theta = 0) = S_0$, is equivalent to a trapping probability in the intrinsic precursor state (monomer species on the bare surface). Using this model, experimental uptake was fitted at submonolayer region, and S_0 was estimated to be 0.46. Fitted curve is shown as dashed curve in Fig. 6.1. This result is comparable with the previous report: $S_0 = 0.58$ for H_2O/Rh(111).[4]

Sticking is a dynamic phenomenon. When a water molecule incomes to the surface, it is accelerated by the attractive chemisorption potential and scattered by the corrugated potential at the surface. This causes various excitations including rotation, vibration, and translation. In addition, adsorption energy must be dissipated to the substrate via electron-hole pair (EHP) and phonon excitations in order to be trapped by a chemisorption potential well.[22] The enhancement of the phonon excitation results from the increasing mass ratio of water to metal atoms; Ru > Rh > Pt (mass Ru = 101.1 g/mol, mass Rh = 102.9 g/mol, mass Pt = 195.1 g/mol). However, S_0 of Ru(0001) and Pt(111) surfaces was estimated to be unity, whereas that of Rh(111) is 0.46 estimated in this study.

In addition, I think that lattice constant of these surface could affect the smaller S_0 of Rh(111). As a water molecule income to the surface, it must orient

the molecular plane parallel to the surface to feel a strong attractive force. Electronic coupling between molecule and substrate induces the EHP excitation, and thus increases the adsorption probability. Here the lattice constant of Rh(111) is smaller than that of Ru(0001) and Pt(111), and theoretical calculation predicted that the adsorption energies of monomer species are in the sequence: Pt(111) < Ru(0001) < Rh(111).[23] Thus multi-dimentional potential energy surface (PES) of water/Rh(111) may be more corrugated than that of Ru(0001) and Pt(111). Greater the corrugation of PES that a molecule feel, less molecules would reorient rapidly to chemisorption alignment on the timescale of a collision.[24] Thus, I think that an incoming water molecule is less efficiently scattered inelastically inducing EHP excitations by the Rh(111) surface compared with the Ru(0001) and Pt(111) surfaces.

6.3.2 Desorption kinetics

6.3.2.A Coverage dependence of TPD spectra

In the thermodynamic equilibrium condition, desorption should occur as a reverse process of adsorption. A series of TPD spectra of D_2O adsorbed on Rh(111) were measured as a function of water exposure [Fig. 6.3 (a)]. Water molecules were adsorbed on Rh(111) at 20 K, and then annealed at 145 K. Note that no difference was observed, in the epitaxially grown layer at 145 K, with a constant flux of ~0.01 (fractional coverage)/s.

At θ=0.013, the TPD spectrum consists of the two broad peaks around 171 and 180 K, of which the former develops as coverage increases. The latter small peak at 180 K soon becomes saturated, which may be due to the small amount of defects (steps and kinks). Assuming that the fractional coverage θ=1.0 is equal to 1 BL (2/3 ML) and that water molecules are adsorbed on the step sites as molecular chains,[25] the amount of defects on the Rh(111) surface is

estimated to be less than 0.5%. Note that, judging from IRAS, water molecules were not dissociated by the defects.

A series of TPD spectra of the first layer shows a large peak with a desorption maxima at 171 ~ 180 K. On the other hand, the inset of Fig. 6.3(a) shows water desorption from the oxygen preadsorbed Rh(111) surface, where oxygen molecules were adsorbed at 20 K followed by annealing to 300 K ($\theta_O \cong 0.06$ ML). Here, the O–preadsorbed Rh(111) surface was exposed to water at 20 K, and then annealed at 155 K for 60 s. In the TPD spectrum, two desorption maxima are observed at 164 and 202 K. Previously, Wagner and Moylan[26] reported that, in the presence of oxygen, some water molecules were dissociated to form adsorbed hydroxyl species on Rh(111). The high temperature TPD peak is due to the disproportionation reaction of the hydroxyl species and the desorption of intact water molecules associated with hydroxyl species. On the "clean" Rh(111) surface, only one desorption peak is observed in submonolayer coverages, except for a very small defect derived peak. Therefore, I conclude that water molecules adsorb and desorb intact on Rh(111). Note that no strong isotope effect, as was reported for water on Ru(0001)[21], was observed in TPD of H_2O and D_2O on Rh(111) (not shown here).

At $\theta \leq 1.0$, TPD spectra show the following features: (1) Desorption curves do not show any common leading (low temperature) edge. (2) With increasing coverage, the desorption peak maxima shift to higher temperatures. (3) The peak shape is asymmetrical. (4) At $\theta \geq 0.85$, a small shoulder is observed at the leading edge region [indicated by an arrow at ~162 K in Fig. 6.3(b)]. The small shoulder observed at ~162 K is not a multilayer feature, but due to the first water layer on Rh(111), because the water layer was annealed at 145 K in order to desorb the multilayer before TPD measurement. Thus, a small amount of less stable species may exist near the saturation coverage, suggesting that the structure of the first water layer changes with increasing coverage above $\theta = 0.85$.

These results, (1) ~ (3), indicate that the desorption is not the case of

integral order desorption. Figure 6.4 shows simulated TPD spectra as a function of coverage, where E_d and ν are assumed to be constant. For a zero-order desorption process, the temperature for the desorption maximum shifts to higher temperature with increasing coverage and all desorption curves have a common leading edge [Fig. 6.4(a)]. For a first-order process, with increasing coverage, the maximum of a desorption curve remains at a constant temperature [Fig. 6.4(b)]. For a second-order process, the desorption spectra show a shift in peak maxima to lower temperatures with increasing coverage and the peak shapes remain symmetrical [Fig. 6.4(c)]. These features do not satisfy the observed results, (1)~(3).

Intuitively, I think, in this system, that the desorption rate is proportional to the square root of coverage. When water molecules are adsorbed on the Rh(111) surface, they form 2D islands via the hydrogen bond network at submonolayer coverage[26,27] (see also chapter 6). As a reverse process, desorption occurs from the island edge because the water molecules situated there may be less stable than those in the island due to the lack of one hydrogen bond. Note that, the number of water molecules at the island edge is proportional to the square root of coverage assuming that disc-like 2D islands are formed. Thus, the order of desorption is half in this desorption process because of island geometrical effect. Figure 6.4(d) shows simulated half-order TPD spectra. Half-order desorption kinetics accounts for the observed features of (1) ~ (3).

In this desorption mechanism, the rate limiting step is a detachment from 2D island edge. Based on this desorption process, water molecules adsorbed lately should attach at the island edge thus they should desorb in first. This assumption could be clarified by TPD experiment using isotopic water molecules. Water molecules ($H_2{}^{16}O$) were adsorbed on the Rh(111) surface at 145 K followed by adsorption of $H_2{}^{18}O$ at 85 K, where fractional coverage of $H_2{}^{16}O$ and $H_2{}^{18}O$ are 0.3 and 0.2 respectively. TPD spectrum is shown in Fig. 6.5. Similar

TPD spectrum shape is observed which indicate that these species were situated at similar environment. Thus, fast exchange of $H_2{}^{16}O$ (inside of island) and $H_2{}^{18}O$ (edge of island) should occur before desorption. This result is conflict with an intuitive assumption, because $H_2{}^{18}O$ should desorb first compared to $H_2{}^{16}O$ to explain fractional order desorption by geometrical effect. Thus, water desorption should be explained by the other mechanism.

Typically, quasiequilibrium can be maintained if the energetic barriers between various configurations of the adsorbed layer are small compared to the energy scale for desorption so that the time scale for desorption is long compared to the time scale for the adsorbed layer to equilibrate at a given coverage. In the case of water/Rh(111) system, adsorption energy of monomer and 2D bilayer is calculated to about 36 and 56 kJ/mol,[28] and entropy gain out of condensed phase into dilute phase may be very large. Thus, quasiequilibrium between condensed (solid or liquid) and dilute (gas on bare surface and condensate) phase in 2D may be maintained in this system, and this can explain the observed TPD result; fast exchange of $H_2{}^{16}O$ and $H_2{}^{18}O$ before desorption.

In such a situation, however, there will be a coverage regime where the desorption kinetics is roughly zero order in thermodynamic argument. Here, note that the zero order desorption needs assumptions that sticking probability on the bare and condensate surface is same.[29] The quasiequilibrium between condensed and dilute phase implies, from the equality of the chemical potentials, equal vapor pressures for both phases, and then go on to assume that this implies equal desorption rates from both phases. Even if the vapor pressure are equal, desorption rates from both phase can only be equal if the sticking probabilities on the dilute and condensed phases are equal. In this system, D_2O/Rh(111), I estimated the sticking probabilities of the bare and 2D island surfaces to be 0.46 and 1, respectively. Thus the desorption rate should depend on the coverage.

H. J. Kreuzer and S. H. Payne reported the desorption from a two-phase

(gas and solid in 2D) adsorbate with different sticking probabilities in theory.[29] In their model, they treated the 2D gas as an ideal and approximated the condensed phase by an Einstein model, but qualitative arguments would be adaptable. They reported the simulated isothermal desorption [Fig. 6.6(a)] and TPD spectra [Fig. 6.6(b)] for different sticking probabilities on bare (S = 0.6) and 2D island (S = 1.0) using mean field approximation (treat the adsorbate/adsorbate interactions in an average sense) with parameters chosen for Xe/Ni(111). Within the coexisting region, the area of the condensed (dilute) phase increases (decreases) linearly as coverage builds up while the density in the two-phases, and the partial sticking probabilities on either, remain constant. Thus, the desorption order is unity within the coexisting region, which can be shown in Fig. 6.6(a). Dashed lines means upper and lower coexistence points. The corresponding traces for TPD are shown in Fig. 6.6(b). The observed spectrum features in this study, (1)~(3), agree well with Fig. 6.6(b).

In addition, simulated TPD spectra show a small shoulder at the leading edge region. This feature was also observed in this study as noted (4) above. This is due to a rapid increase in chemical potential of adsorbate as the condensate density is compressed from its value in the coexisting region. Thus, observed features of TPD spectra, (1)~(4), could be explained qualitatively with their model, I conclude that, in this system, apparent fractional order TPD spectrum shape is derived from the difference of sticking probability on the bare and condensed phase, and desorption order is unity in the coexisting region.

6.3.2.B Desorption activation energy and preexponential factor

In this section, kinetic parameters of desorption, the activation energy (E_d) and the preexponential factor (ν_d), were estimated as a function of coverage. Analytical methods used for TPD spectra can be categorized into two groups: an integral approach and a differential approach respectively (see section 3.3). The

former utilizes peak characteristics to extract coverage–independent kinetic parameters from a single desorption peak.[30–32] On the other hand, the latter is used to extract coverage–dependent kinetic parameters and this method is sometimes even applied for multiple overlapping desorption curves. In this study, I use the differential approach, i.e., the threshold temperature programmed desorption (TTPD) method,[33,34] because the activation energy can be estimated as a function of θ without assuming the desorption order. This method utilizes the desorption rate vs. temperature data from the onset of a low temperature tail (the threshold region) of a single desorption spectrum to prepare an Arrhenius–type plot. The slope and the intercept of each Arrhenius plot provide the E_d and ν_d, respectively.

Since water molecules adsorb and desorb intact on Rh(111), we assume that the desorption order is unity and zero for the submonolayer and multilayer, respectively. When the pumping speed of the system is sufficient to render readsorption negligible, the mass spectrometer ion current signal is proportional to the desorption rate.[30] This proportion is constant, determined by the integrated TPD peak area at a full coverage, assuming that the fractional coverage, θ=1.0, is equal to absolute coverage 1.0 BL (2/3 ML). In the present TTPD analysis, the threshold coverage increments used for $0<\theta<0.68$ and $0.68<\theta<1.0$ spectra are below 5% and 1%, respectively; and I assume that neither E_d nor ν_d vary significantly within these coverage increments. This assumption is justified by the linearity of the Arrhenius plots as shown in Fig. 6.7.

Figure 6.8(a) shows the E_d as a function of water coverage. E_d is estimated to be 60 kJ/mol at θ=0 and is nearly constant to θ~0.6. This activation energy is higher than the values previously reported (~42 kJ/mol) for H_2O desorption, which were obtained in the limit of zero coverage, assuming a first order desorption and a preexponential factor of 10^{13} s^{-1}. [1,4,20] As the water coverage increases, E_d decreases gradually until θ=1.0, where E_d reaches 51 kJ/mol. For multilayer desorption [see Fig. 6.3(a)], E_d was estimated to be 55

kJ/mol, which is in agreement with the previous measurement (50.46 kJ/mol).[35] Here, E_d at $\theta \leq 0.6$ is larger than that of the multilayer. Therefore, the energetic stabilization of water adsorbed in the first layer, compared to the multilayer, is clear evidence that water wets the Rh(111) surface. Note that the activation energy for desorption near the saturation coverage is slightly less than that of the multilayer.

With an integral approach, it is difficult to estimate the preexponential factor as a function of θ. However, the variation of ν_d with respect to coverage is very informative in understanding the equilibrium and the rate process. Using the TTPD method, the preexponential factors are estimated as a function of water coverage, assuming first-order desorption [Fig. 6.7(b)]. ν_d is estimated to be 4.1×10^{17} s^{-1} at $\theta=0$ and is nearly constant to $\theta \sim 0.6$. With coverage further increased, ν_d decreases to be 1.3×10^{14} s^{-1} at the saturation coverage. For multilayer desorption, which is a zero-order process, ν_d is estimated to be 3.2×10^{16} ML/s, which is in good agreement with the previous measurement of crystalline water ice (1.02×10^{16} ML/s).[35] In the first layer desorption, the preexponential factor varies by more than 10^3 as a function of coverage, indicating that the effective stabilization of the first water layer at higher coverages ($\theta \geq 0.6$) originates from the decrease in the preexponential factor. A significant change in ν_d as a function of coverage has also often been observed.[36]

In the theory of the absolute reaction rate, the preexponential factor is related to the entropy of an activated process [$\nu = (kT/h)\exp(\Delta S/R)$ for first-order process, where T is the absolute temperature, h the Planck constant, ΔS the entropy of activation, and R the gas constant. Here, the transmission coefficient is assumed to be unity].[37] Since gaseous water molecules adsorb on Rh(111) through a non-activated process, the entropy of desorption is considered as the entropy difference between the gas phase and adsorption states, based on the principle of detailed balance at equilibrium. Therefore, a large preexponential factor (4.1×10^{17} s^{-1}) indicates a low entropy adsorption state. Up to $\theta \sim 0.6$, the

preexponential factor is nearly constant. These results indicate the water layer forms an ordered structure, which is related to the $\sqrt{3}$ phase, even at low θ (see chapter 7), and the adsorption structure may not change with increasing coverage up to θ~0.6. However, the preexponential factor gradually decreases above θ~0.6. This indicates that the water layer at $\theta \geq 0.6$ has a higher entropy than that at $\theta \leq 0.6$. Generally, the entropy of the adlayer is given by both the internal entropy for each adsorbed molecule and the configurational entropy in the 2D layer, i.e. the entropy associated with the arrangement of adsorbed molecules on the surface. These results may be consistent with LEED and IRAS results, which will be discussed in chapter 7.

Similar coverage dependence of E_d and ν_d in Fig. 6.8 is due to a well-known compensation effect[38]; whereby at a certain coverage, the preexponential factor and the desorption activation energy follows the Arrhenius relation $\ln\nu_d = E_d/RT_c + c$, where c is a constant and T_c is a characteristic temperature. In the present experiment, we obtained a straight line for $\ln \nu_d$ vs. E_d with T_c=163 K. The compensation effect is common in many desorption systems.[36] Niemantsverdriet et al.[39] have shown that the compensation effect can drastically influence the desorption spectrum of an adsorbate system with pairwise lateral interactions. It is emphasized that,[39] due to the compensation effect, desorption analysis procedures based on peak maximum temperature and peak width (integral method) always lead to incorrect results.[40] According to their report, T_c=163 K, as I obtained here, indicates a relatively strong compensation effect. Therefore, it is reasonable to use the TTPD analysis procedure in the present study.

6.4 Conclusion

In summary, adsorption and desorption kinetics of water molecules on the Rh(111) surface were investigated using TPD. Water molecules show a coverage dependent sticking probability and S_0 was estimated to be 0.46. In desorption process, water molecules exhibit coexistence of a dilute, gas like phase together with islands of a condensed phase, both being two dimensional. Based on the model proposed by K. J. Kreuzer and S. H. Payne,[29] apparent fractional-order TPD peak shape can be attributed to a first-order desorption with two phases on the surface. Using TTPD method, coverage dependence of E_d andν_d were estimated. They showed weak coverage dependence, where E_d and ν_d were decreased from 60 kJ/mol to 51 kJ/mol and from 4.1 x 10^{17} s^{-1} to 1.3 x 10^{14} s^{-1} with increasing coverage, respectively.

Figures and Table

substrate	water	S_0	T(K)	method	coverage dependence of S	note	Ref.
Ice	H_2O	1	<130	molecular beam	×	Ice films on Ru(0001)	[3]
Pt(111)	D_2O	0.7	55~150	TPD	×		[5]
	H_2O	0.7	100	TPD	×		[6]
	H_2O	0.2	130~147	STM	O		[7]
	H_2O/D_2O	1	138~144	molecular beam	×		[8]
Pt(100)	H_2O	1	150	TPD	×		[9]
Ru(0001)	H_2O	1	95	TPD	×	partial dissotiation	[10]
Rh(111)	H_2O	0.58	100	TPD	×		[4]
	D_2O	0.46	135	TPD	O		The present study
Pd(100)	H_2O/D_2O	0.22	10	HREELS			[11]
Ni(110)	H_2O	1	80	UPS	O		[12]
Au(111)	H_2O	0.95	85	molecular beam	×		[13]
Cu(100)	H_2O/D_2O	0.12	10	HREELS			[11]
Cu(110)	H_2O	1	110	TPD	×		[14]

Table 6. 1. Measured or estimated initial sticking probabilities for water on metals. T(K) is an adsorption temperature.

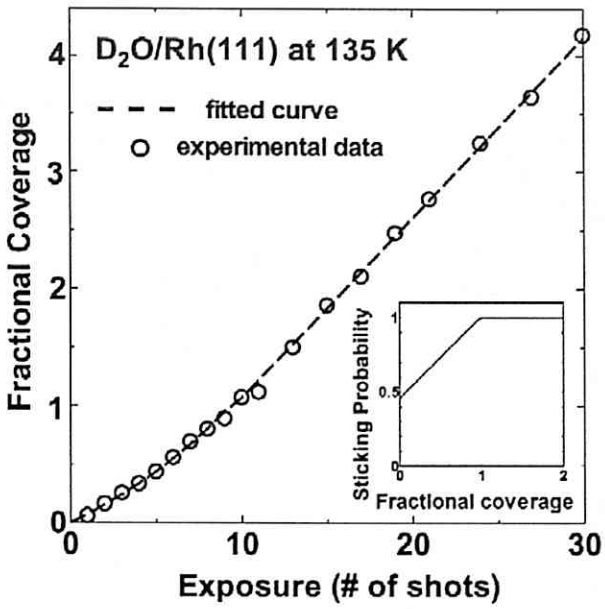

Fig. 6. 1. Exposure dependence of adsorbed water coverage. Water molecules were adsorbed at 135 K followed by TPD measurement. Dashed curve is fitted assuming that the S on the 2D islands is unity. By fitting the submonolayer region, S_0 was estimated to be 0.46.

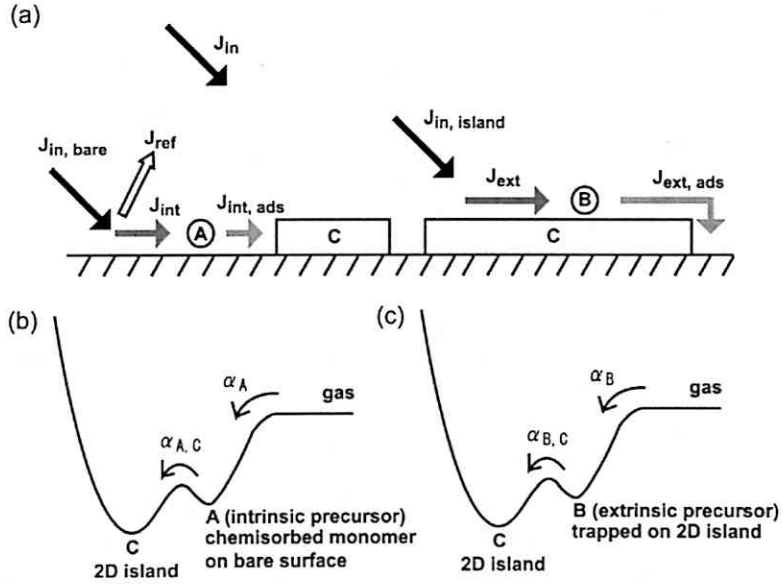

Fig. 6. 2. (a) Representation of the water fluxes in this experiment. Each notation is explained in text. (b) One-dimentional schematic illustration of adsorption process for water molecules impinged on the bare surface. (c) One-dimentional schematic illustration of adsorption process for water molecules impinged on the 2D island.

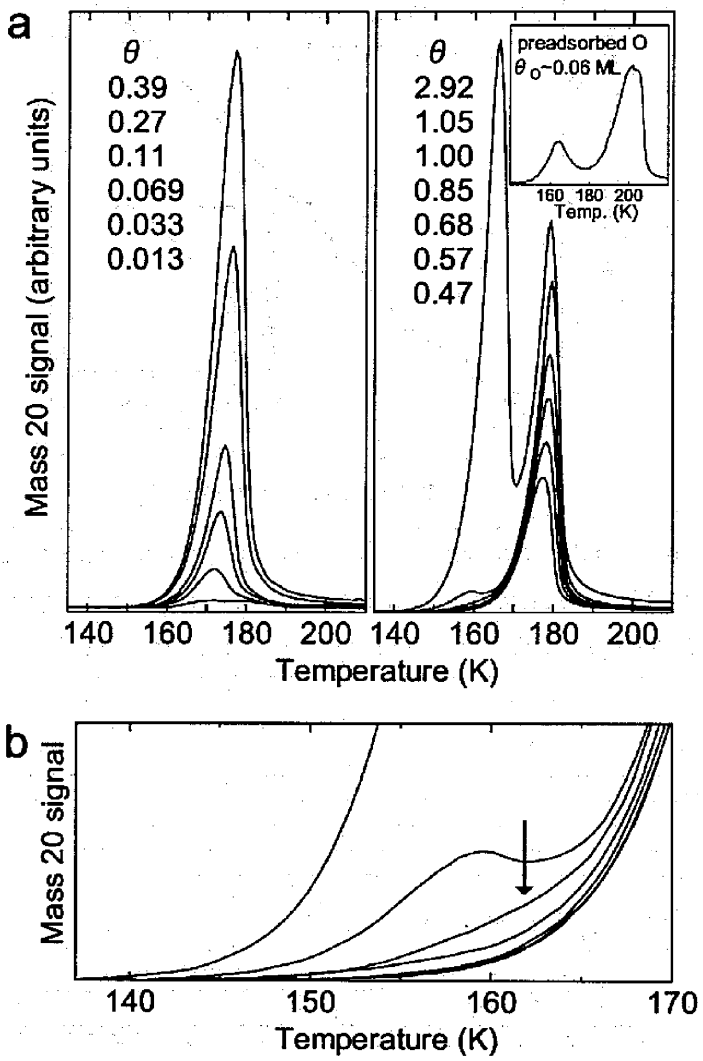

Fig. 6. 3. (a) Temperature programmed desorption spectra of D_2O on the clean Rh(111) surface, with a heating rate of 1.3 Ks^{-1}. Water molecules were adsorbed on Rh(111) at 20 K, then annealed at 145 K. The water coverage of each spectrum is shown in the figure. Left: the low coverage region from 0.013 to 0.39. Right: the high coverage region from 0.47 to 2.92. The effect of preadsorbed oxygen is shown in the inset. Oxygen molecules were adsorbed at 20 K followed by annealing to 300 K. After cooling to 20 K, the O/Rh(111) surface was exposed to water, and then annealed at 155 K for 60 s. The coverage of preadsorbed oxygen atom was about 0.06 ML and a heating rate was 0.71 Ks^{-1}. (b) The leading edge region of TPD spectra for $0.47<\theta<2.92$. At $\theta \geq 0.85$, a small shoulder was observed at the leading edge region (indicated by an arrow at ~162 K).

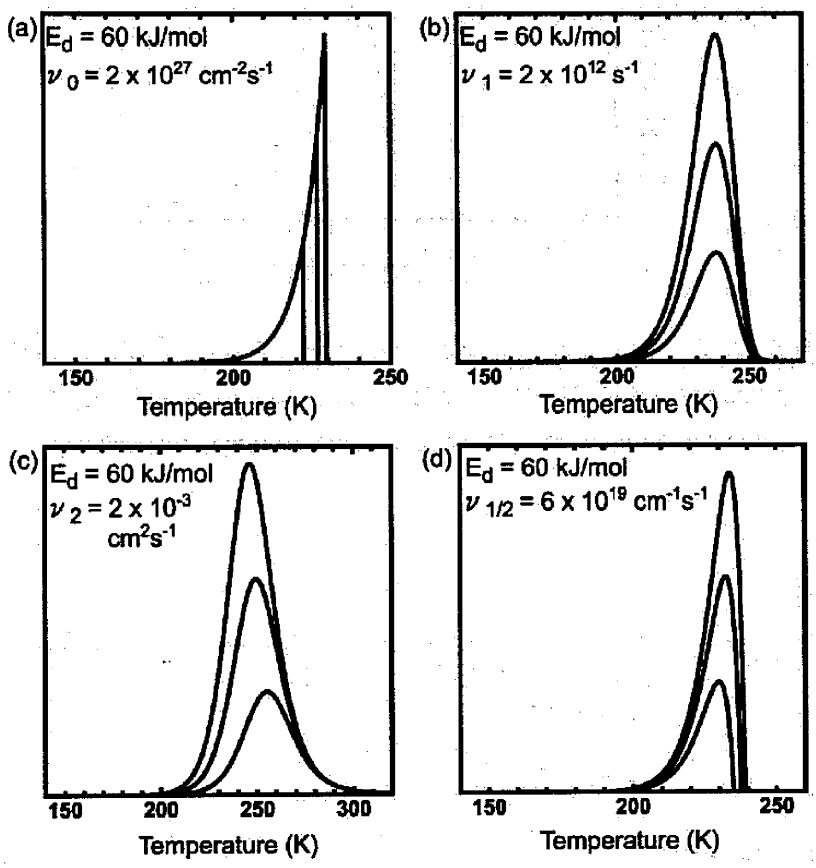

Fig. 6. 4. Simulated TPD spectra assuming that kinetic parameters [(desorption activation energy (E_d) and preexponential factor (ν)] are independent of coverage. Heating rate is 1.0 Ks^{-1}. (a) zero-order, (b) first-order, (c) second-order and (d) half-order. For n-th order desorption, preexponential factor, ν_n, is assumed to be typical value.

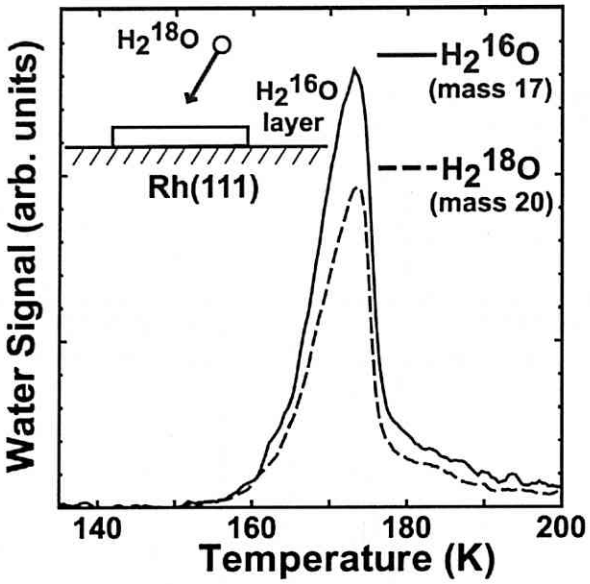

Fig. 6. 5. TPD spectra of coadsorbed isotopic water ($H_2{}^{16}O$ and $H_2{}^{18}O$) on the Rh(111) surface with a heating rate of 1.3 K s^{-1}. $H_2{}^{16}O$ was adsorbed at 145 K followed by $H_2{}^{18}O$ adsorption at 85 K. These spectra were normalized by that at saturation coverage, respectively.

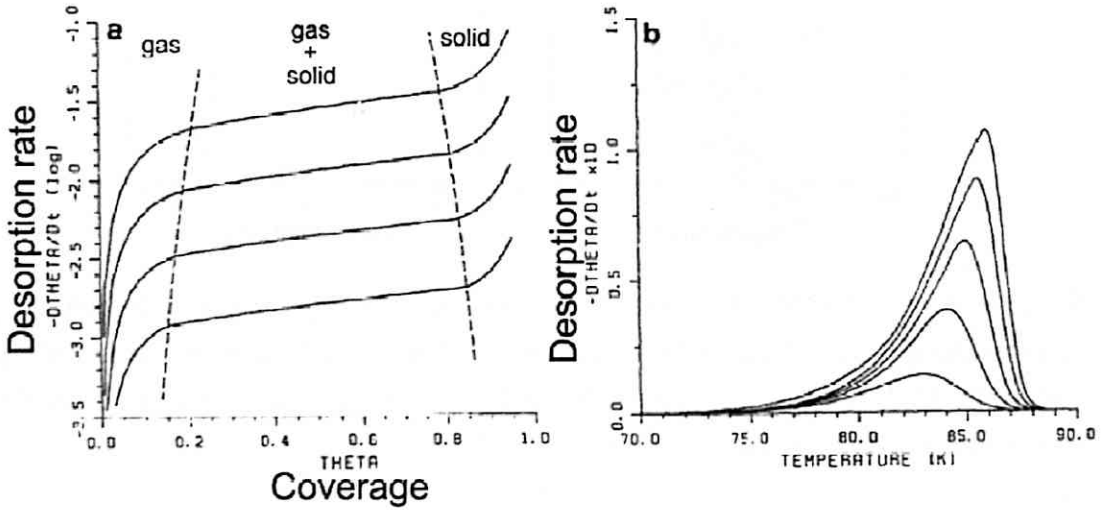

Fig. 6. 6. Simulated results calculated by H. J. Kreuzer and S. H. Payne.[29] (a) Isothermal desorption for varying temperature (top to bottom) T = 82, 80, 78, 76 K. Parameters approximating Xe/Ni(111), see original paper. Dashed lines show coexistence boundaries. (b) Corresponding TPD traces with heating rate 0.5 Ks^{-1} and initial coverages (top to bottom) θ_0 = 0.95, 0.75, 0.55, 0.35, 0.15.

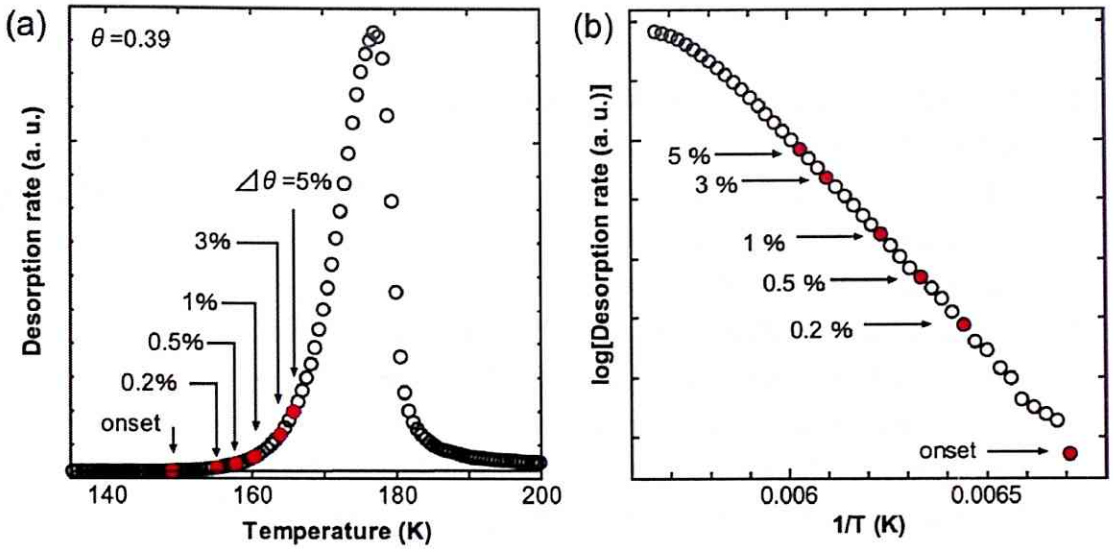

Fig. 6. 7. (a) TPD spectrum for θ = 0.39 D_2O/Rh(111), (b) Arrhenius plot for D_2O/Rh(111) TTPD at θ = 0.39.

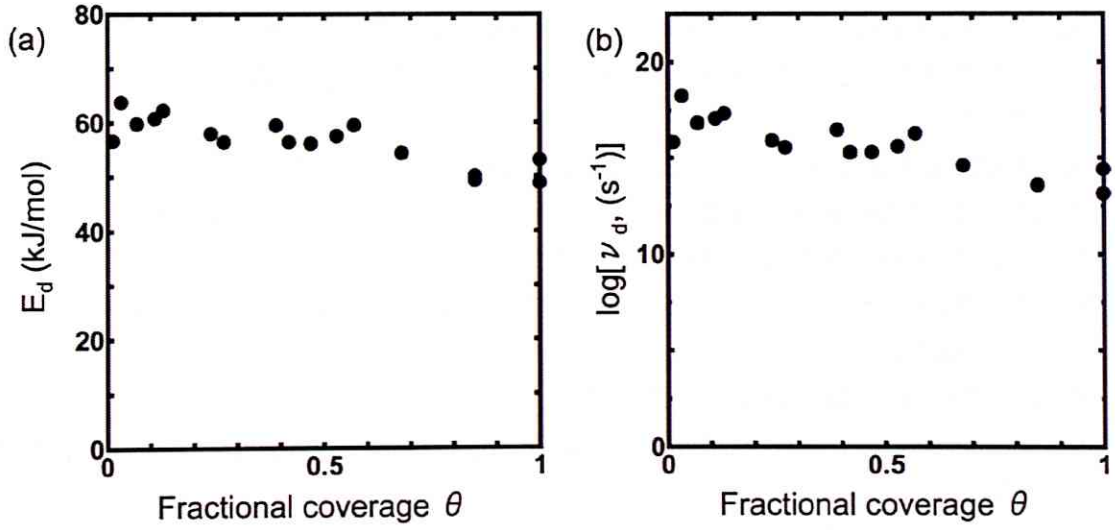

Fig. 6. 8. (a) Desorption activation energy as a function of water coverage. (b) Preexponential factor for water desorption as a function of coverage. I assume that the desorption order is first.

References

1. P. A. Thiel and T. E. Madey, Surf. Sci. Rep. **7**, 211 (1987).
2. M. A. Henderson, Surf. Sci. Rep. **46**, 1 (2002).
3. D. E. Brown, S. M. George, C. Hung, E. K. L. Wong, K. B. Rider, R. S. Smith, and B. D. Kay, J. Phys. Chem. **100**, 4988 (1996).
4. J. J. Zinck and W. H. Weinberg, J. Vac. Sci. Technol. **17**, 188 (1980).
5. S. K. Jo, J. Kiss, J. A. Polanco, and J. M. White, Surf. Sci. **253**, 233 (1991).
6. G. B. Fisher, Monolayer and Multilayer Adsorption of Water on the Pt(111) Surface, General Motors Research Publication No. GMR-4007/PCP-171 (1982).
7. M Morgenstern, J. Muller, T. Michely, and G. Comsa, Z. Phys. Chem. **198**, 43 (1997).
8. S. Haq, J. Harnett, and A. Hodgson, Surf. Sci. **505**, 171 (2002).
9. H. Ibach and S. Lehwald, Surf. Sci. **91**, 187 (1980).
10. P. A. Thiel, F. M. Hoffmann, and W. H. Weinberg, J. Chem. Phys. **75**, 5556 (1981).
11. S. Andersson, C. Nyberg, and C. G. Tengstal, Chem. Phys. Lett. **104**, 305 (1984).
12. K. Jacobi and H. H. Rotermund, Surf. Sci. **133**, 401 (1983).
13. B. D. Kay, K. R. Lykke, J. R. Creighton, and S. J. Ward, J. Chem. Phys. **91**, 5120 (1989).
14. K. Bange, D. E. Grider, T. E. Madey, and J. K. Sass, Surf. Sci. **137**, 38 (1984).
15. M. Klaua and T. E. Madey, Surf. Sci. **136**, L42 (1984).
16. C. T. Au, J. Breza and M. W. Roberts, Chem. Phy. Lett. **66**, 340 (1979).
17. J. L. Daschbach, B. M. Peden, R. S. Smith, and B. D. Kay, J. Chem. Phys. **120**, 1516 (2004).
18. C. Clay, L. Cummings and A. Hodgson, Surf. Sci. **601**, 562 (2007).
19. M. E. Gallagher, S. Haq, A. Omer and A. Hodgson, Surf. Sci. **601**, 268 (2007).
20. R. H. Stulen and P. A. Thiel, Surf. Sci. **157**, 99 (1985).
21. N. S. Faradzhev, K. L. Kostov, P. Feulner, T. E. Madey, and D. Menzel, Chem. Phys. Lett. **415**, 165 (2005).
22. J. C. Tully, Surf. Sci. **299/300**, 667 (1994).
23. Michaelides, V. A. Ranea, P. L. de Andres, and D. A. King, Phy. Rev. Lett. **90**, 216102 (2003).
24. J. T. Kindt and J. C. Tully, Surf. Sci. **477**, 149 (2001).
25. M. L. Grecea, E. H. G. Backus, B. Riedmüller, A. Eichler, A. W. Kleyn, and M. Bonn, J. Phys. Chem. B. **108**, 12575 (2004).
26. F. T. Wagner and T. E. Moylan, Surf. Sci. **191**, 121 (1987).
27. S. Yamamoto, A. Beniya, K. Mukai, Y. Yamashita, and J. Yoshinobu, J. Phys. Chem. B. **109**,

5816 (2005).

28. P. Vassilev, R. A. van Santen, and M. T. M. Koper, J. Chem. Phys. **122**, 054701 (2005).
29. H. J. Kreuzer and S. H. Payne, Surf. Sci. **200**, L433 (1988).
30. P. A. Redhead, Vacuum. **12**, 203 (1962).
31. C. M. Chan, R. Aris, and W. H. Weinberg, Appl. Surf. Sci. **1**, 360 (1978).
32. D. Edwards, Jr., Surf. Sci. **54**, 1 (1976).
33. E. Habenschaden and J. Küppers, Surf. Sci. **138**, L147 (1984).
34. J. B. Miller, H. R. Siddiqui, S. M. Gates, J. N. Russel, Jr., J. T. Yates, Jr., J. C. Tully, and M. J. Cardillo, J. Chem. Phys. **87**, 6725 (1987).
35. R. J. Speedy, P. G. Debenedetti, R. S. Smith, C. Huang, and B. D. Kay, J. Chem. Phys. **105**, 240 (1996). In this report, 1 ML is defined as an ice monolayer on Ru(001).
36. E. G. Seebauer, A. C. F. Kong, and L. D. Schmidt, Surf. Sci. **193**, 417 (1988).
37. S. Glasstone, K. J. Laidler, and H. Eyring, *The theory of rate processes: the kinetics of chemical reactions, viscosity, diffusion and electrochemical phenomena*, (McGraw–Hill, New York, 1941).
38. G. A. Somorjai, *Chemistry in two dimensions: Surfaces*, (Cornell University Press, Ithaca, 1981).
39. J. W. Niemantsverdriet, K. Markert, and K. Wandelt, Appl. Surf. Sci. **31**, 211 (1988).
40. J. T. Yate, Jr., P. A. Thiel, and W. H. Weinberg, Surf. Sci. **84**, 427 (1979).

Chapter 7

The first water layer and thin film growth on the Rh(111) surface

The adsorption states and growth process of the first water (D_2O) layer and multilayer on Rh(111) were investigated using IRAS, TPD, and SPA–LEED. At the initial stage, water molecules form the commensurate ($\sqrt{3}x\sqrt{3}$)*R*30° structure. This two-dimensional structure is flatter than the ice-like bilayer consists of the D-down species. The D-down domains show a characteristic island shape. With increasing coverage, ice-like bilayer (D-up) grows and shows a incommensurate structure. At nearly the saturation coverage, the ice-like bilayer is ~9 % compressed from the commensurate ($\sqrt{3}x\sqrt{3}$)*R*30° structure, which is ~5% compression with respect to ice I_h. At saturation coverage, the first water layer consists of the ice-like bilayer (D-up) and flat (D-down) domains, where the D-up domains occupy 44 % and the D-down domains occupy 56 % in coverage. Further adsorption of water molecules form three-dimensional ice crystallites on the D-down domains where the D-down species do not reorient to accommodate formation of a crystalline ice.

7.1 Introduction

When water molecules adsorb on a metal surface, they interact with the surface through van der Waals, charge transfer and/or hydrogen bond interactions. Water molecules have been observed on surfaces in the form of monomers, dimers, larger clusters, two–dimensional (2D) bilayers, and three–dimensional (3D) islands.[1,2] In these adsorbed states, the ordered 2D overlayers were investigated most intensively.[1,2] However, despite many experimental and theoretical studies, there remain open questions: of which the most relevant involves a geometric structure and the behavior of the first water layer on close–packed transition metal surfaces. Besides the structure of the first water layer, much less is known about the morphology of nanometer scale water films. In this study, the adsorption states and growth process of the first water (D_2O) layer and multilayer on Rh(111) were investigated.

In section 1.2, the proposed models of the first water layer on a metal surface are mentioned; ice-like bilayer (H-up)[3], compressed bilayer (H-up)[4,5], H-down[6], and half-dissociated model[7]. The H-down model was proposed for the water adlayer on the Pt(111) surface, the other models are proposed for that on the Ru(0001) surface.

To reveal whether water molecules dissociatively adsorb or not on Ru(0001), many experimental studies have been performed.[8–15] However, recent experimental studies have reached opposing conclusions. Using x–ray photoelectron spectroscopy (XPS), Weissenrieder *et al.*[8] reported that the stable wetting layer of water on Ru(0001) contains OH and H_2O in roughly 3 : 5 proportions below 170 K. On the other hand, other XPS,[9-11] infrared reflection absorption spectroscopy (IRAS), together with temperature programmed desorption (TPD)[12] and LEED[13], indicate that water molecules wet the Ru(0001) surface intact. Based on vibrational spectra, Denzler *et al.*[14] reported that water

molecules on Ru(0001) were arranged as the D-down model. These contradictory results might be due to different experimental conditions. Andersson *et al.*[9] reported that the dissociation was an activated process and kinetically forbidden at low temperatures (≤140 K). In addition, it was reported that the dissociated layer observed experimentally[8] may be derived from the extreme sensitivity of the water layer to electron or x–ray irradiation, electron impact leads to water dissociation with very high cross-sections (in the high 10^{-16} cm^2 range at 100-200 eV) and low threshold energies on the Ru(0001) surface.[10] Therefore, non–destructive experiments are crucial to study water adsorption on metal surfaces.[10,11,13]

As mentioned above, water molecules wet Pt(111) and Ru(001) intact (≤140 K). Recent experiments have shown that the first water layer on Pt(111)[6,15] and Ru(0001)[13,14] are arranged with the H-down species, where the H-up species rarely exist.

In the H-down model proposed by Ogasawara *et al.*, water molecules are arranged as the commensurate $(\sqrt{3}x\sqrt{3})R30°$ geometry, where all water molecules are situated at on-top sites.[6] However, two different phases, $(\sqrt{37}\times\sqrt{37})R25.3°$ at low coverage and $(\sqrt{39}\times\sqrt{39})R16.1°$ at high coverage, were observed at temperature above 135 K using LEED[15] and diffraction of He atom[16]. Models of these structures are shown in Fig. 7.1. Here the 2D lattice of $(\sqrt{37}\times\sqrt{37})R25.3°$ structure is expanded slightly by 4.4 % and that of $(\sqrt{39}\times\sqrt{39})R16.1°$ structure is compressed by 3.3 %, compared to the basal plane of ice I_h, respectively. On the other hand, three different structures were observed using a STM (scanning tunneling microscopy), these structures are depending on the preparation conditions (temperature and water vapor exposure), and are different in molecular density.[18] And thus, controversy still exists in the literature regarding the structure of first water layer on Pt(111).

In the case of Ru(0001), Haq *et al.*[13] have reported that water adsorption creates flat lying (molecular plane is parallel to the surface) clusters, rather than

extended islands, preferring to optimize the Ru-water interaction at the expense of a reduced hydrogen bonding configuration. Only as the coverage increases towards 0.67 ML, the film order into the $(\sqrt{3}\times\sqrt{3})R30°$ structure where water buckles out of plane into an H-down geometry. Adsorption continues past the ordered 0.67 ML structure to saturate with a coverage of 0.76 ML, with some of the additional water adsorbed in the H-up geometry.

Similar model was proposed by Mitsui *et al.* for submonolayer water on the Pd(111) surface.[19] They observed the aggregation of water leads to the formation of hexagonal honeycomb structures in registry with the Pd(111) substrate below 130 K. The lateral growth of these clusters is limited to a few unit cells, as shown in Fig. 7.2. On the basis of this result, they proposed a model where the molecules are nearly coplanar and use their hydrogen atoms to form bonds with neighboring molecules, while bonding to the substrate through the lone pair orbitals. This model implies necessarily that the cluster size must be limited to a few cells since in two dimensions only a finite number of molecules can be fully hydrogen bonded (double donors, single accepter, and a forth bond to the substrate). They also found this structures are metastable: when the sample was heated to 130 K, the structure changed considerably. Table 7.1 shows the experimental results of molecular wetting structures on transition metal surfaces.

On the other hand, based on theoretical studies, the adsorption energies of the H-up and H-down models are nearly the same on transition metal surfaces.[17,20-23] These theoretical results suggest that water molecules could exist as a mixture of the H-up and H-down models in real systems. However, no experimental studies supporting the mixture of H-up and H-down models have yet been reported.

Besides the structure of first water layer, much less is known about the growth mechanism of nanometer scale water films (e.g., coverages greater than 1 BL). The influence of the first water layer on the growth morphology of ice films

has recently been demonstrated on Pt(111), where H-down (i.e. fully coordinated) configuration of first water layer results in a hydrophobic surface; water molecules form nonwetting 3D ice crystallite on the first water layer.[24,25] Thus, water ice films grow Stranski-Krastanov mechanism (2D layer + 3D islands) on the Pt(111) surface. Same growth mechanism was observed on Pd(111)[25] and Ru(0001)[26,27]. Based on the above idea, hydrophobic first layer, ice crystallite should nucleate randomly on the first water layer. STM measurement; however, showed that the second layer formed a regular pattern of clusters[18], which indicate that there are nucleation sites for multilayer growth. On the other hand, water ice grows layer-by-layer on the Ni(111) surface, where the film orders to form an incommensurate crystalline ice at 2 BL because of weak water-metal interaction (i.e. the first water layer may reconstruct).[28] However the structure of an interface between the fist layer and multilayer is not elucidated, which may strongly influence the growth mechanism of the ice films. Experimental results for multilayer growth mechanism are also shown in table 7.1.

Here, we choose Rh(111) as an underlying substrate. Only a few experimental studies have been reported on the interaction of water molecules with Rh(111).[29–33] Previous studies have reported that water molecules adsorb intact and form an ordered $(\sqrt{3}\times\sqrt{3})R30°$ structure on Rh(111). By DFT calculation, however, Feibelman proposed that the OH fragments, which were formed by impurity atoms, could anchor a 2D water layer to the Rh(111) surface. [34] Therefore, controlling surface impurities/defects is indispensable to study the first water layer on Rh(111).

In this study, I investigated the growth process of the first water layer and multilayer on Rh(111), using IRAS, TPD, and spot–profile–analysis LEED (SPA–LEED). In the chapter 6, I conclude that water molecules adsorb intact on the Rh(111) surface. In addition, energetic stabilization of water adsorbed in the first layer, compared to the multilayer, is elucidated. In this chapter, I aims to

elucidate the microscopic adsorption state of water on Rh(111) as a function of coverage. In the present experiments, I carefully controlled the surface impurities/defects and carried out non- or less-destructive measurements.

7.2 Experiment

The experimental conditions and sample preparation are described in chapter 3. The clean Rh(111) surface was carefully prepared, the carbon and boron impurities were removed by oxidation and flashing.[35] The cleanness was checked by the adsorption behavior of CO[36] and D_2O using IRAS, and TPD of H_2O and D_2O[29,31]; and no dissociated species of water was observed in the present experiments (see below).

Water (D_2O, H_2O) vapor was introduced through a pulse gas dosing system onto the sample surface. The water [$H_2{}^{16}O$ (Milli-Q) and $D_2{}^{16}O$ (Aldrich, isotopic purity 99.96%)] was degassed through several freeze–pump–thaw cycles prior to exposure.

IRAS measurements were performed using an FTIR spectrometer (Bruker IFS66v/S) with a B-doped Si (Si:B) detector (with measurable range: 370–4000 cm^{-1}) or a mercury–cadmium–telluride (MCT; HgCdTe) detector (700–7500 cm^{-1}). All the spectra were taken with 4 cm^{-1} resolution and 500 scans.

The LEED measurements were carried out using a SPA-LEED instrument (Omicron). During a typical measurement period, the total electron dose is ~0.01 electrons per surface Rh atom in this study. LEED observation with a small electron dose is quite important, since water molecules adsorbed on the metal surfaces are easily damaged by low energy electrons.[10,11,13]

7.3 Results and Discussion

7.3.1 The first layer of water on the Rh(111) surface

7.3.1.A LEED

When water molecules were adsorbed on Rh(111) at 20 K, and then annealed at 145 K, the formation of a $(\sqrt{3}\times\sqrt{3})R30°$ LEED pattern (see the inset of Fig. 7.3 at θ=0.23) was observed. Figure 7.3 shows a full–width at half–maximum (FWHM) in a percentage of the first surface Brillouin zone (%SBZ) and an integrated intensity of a (1/3,1/3) LEED spot as a function of water coverage. 100 %SBZ is defined as the distance between the specular beam and the first order Rh spot in reciprocal space, $k = 2\pi/0.27$ nm^{-1}.

Even at low coverage, the $(\sqrt{3}\times\sqrt{3})R30°$ LEED pattern is observed. Thus, water molecules are mobile at 145 K and form a hexagonal *commensurate* 2D domain on the Rh(111) surface. Here, the intermolecular distance must be slightly longer than that in bulk I_h to form the commensurate layer because the lattice constant of Rh(111) is 3% longer than that of I_h. Therefore, the water layer should be flatter than the ice–like zig–zag bilayer.

A peak intensity of a diffracted beam for an island containing N ordered scatterers is proportional to N^2. Consequently, the largest island will influence the shape of the beam profile most strongly, and the FWHM will not refer to the mean diameter of the islands on the surface but will be weighted heavily toward the largest islands present.[37] With increasing coverage, the (1/3,1/3) LEED spot becomes sharper and intensifies, but at $0.2 \leq \theta \leq 0.3$ FWHM and integrate intensity do not change smoothly as a function of coverage. These results indicate that the commensurate $(\sqrt{3}\times\sqrt{3})R30°$ islands initially grow with increasing coverage, but at $0.2 \leq \theta \leq 0.3$ new phases appear except the commensurate $(\sqrt{3}\times\sqrt{3})R30°$ domain.

With further increasing coverage, water molecules show new diffraction spots as shown in Fig. 7.4. Figure 7.4(b) shows LEED image at θ = 0.56, where new spots are observed around (0,0) and halo-like intensities also are observed outside the (1/3,1/3) spots. At nearly the saturation coverage, θ = 0.89, these halo-like intensities are more clearly visible in Fig. 7.4(c) and schematically illustrated in the inset as squares. The position and six-fold symmetry of these spots indicate that there is ~9 % compressed hexagon with respect to $\sqrt{3}a_{Rh}$ and ~8° rotated from $[11\bar{2}]$ direction in the real space. In addition, new spots around (0,0) observed at θ = 0.56 are changed to hexagonal ring at θ = 0.89. Figure 7.4(d) shows a one-dimensional cut along $[11\bar{2}]$ of Fig. 7.4(c). Besides (0,0) and (1/3,1/3) spots, new spots are observed at ~12 %SBZ, which indicated a long rage (~$8a_{Rh}$) domain periodicity along $[11\bar{2}]$ direction. K. D. Gibson *et al.* observed small feature near the specular using diffraction of He atom for H_2O/Rh(111), which indicate the superlattice structure with a repeat distance of ~24 Å (~$9a_{Rh}$).[32] They noted that this feature is always present but the positions and intensities were not fully reproducible.[32]

7.3.1.B IRAS

In order to obtain the microscopic information of the adsorbed states, we measured the vibrational spectra of the water layer, grown on the Rh(111) surface using IRAS. A series of IRAS spectra are shown as a function of water coverage in Fig. 7.5. For the submonolayer region $\theta \leq 1.0$, Fig. 7.5(a), D_2O molecules were adsorbed at 20 K followed by annealing at 145 K. Note that no differences in IRAS were observed in the three preparation methods; (1) D_2O molecules were adsorbed at 20 K followed by annealing at 145 K, (2) Amorphous solid water (ASW) thick film was annealed at 165 K to desorb water molecules, (3) D_2O layer was epitaxially grown with a constant flux of ~0.01

(fractional coverage)/s at 145 K. Thus, I measured the thermodynamically equilibrium adsorption states at 145 K by IRAS. Figure 7.5(b) shows the spectra of epitaxially grown multilayer ice of θ=1.4 and of thick crystalline ice film of θ=119, which was prepared by annealing an ASW multilayer at 165 K to crystallize, respectively.

Firstly, I concentrate on the OD stretching (ν_{OD}) mode because the stretching vibration of water is very sensitive to hydrogen bond formation. At the early stage of water adsorption on Rh(111) (θ≤0.31), water molecules show a sharp peak at 2694 cm^{-1} and broad peaks of around 2540, 2460, and 2200 cm^{-1} [Fig. 7.5(a)].

According to our previous study, the peak at 2694 cm^{-1} was assigned to a free OD stretching mode of water molecules inside the 2D islands.[32] This assignment to the free OD was confirmed by the following experiment, where we exposed the D_2O layer showing the IRAS peak at 2694 cm^{-1} to H_2O molecules at 20 K. As a result, the stretching mode at 2694 cm^{-1} decreased in intensity. Since an H_2O molecule forms a hydrogen bond with a free OD via its oxygen lone pair, H_2O adsorption leads to a fall in the number of free OD. Therefore, this mode corresponds to the stretching vibration of free OD. Note that proton exchange and interlayer mixing[38] between the D_2O layer and post-dosed H_2O molecules was not observed at 20 K. For the case of proton exchange and interlayer mixing, a bending mode of HDO (1370 cm^{-1} for the first layer)[30] and a stretching mode of 2-coordinated free OD (2750 cm^{-1})[39] should be observed in IRAS, respectively, but were not at 20 K, which will be discussed in section D. However, I can not elucidate whether the water molecules which have free OD is at the inside or edge of 2D island by this experiment.

Here, in this study, the peak at 2694 cm^{-1} is reassigned to a free OD at the 2D domain edge as follows. Firstly water layer (θ =0.14) are prepared, Fig. 7.6(a). We exposed the D_2O/Rh(111) to ~1 ML Xe at 20 K, where Xe atoms can adsorb on the water island and the bare Rh(111) surface (discussed later in

section 7.3.2). Xe adsorption may not cause structural change of water islands, because Xe atoms weakly physisorb on the surface. If the "D-up" species is in the 2D island, it may interact with Xe atoms adsorbed on the water island, thus the IRAS peak observed at 2694 cm^{-1} should perturbed by Xe adsorption on the 2D island. Figure 7.6(b) shows an IRAS spectrum of $Xe/D_2O(\theta = 0.14)/Rh(111)$, where the water islands and the bare Rh(111) surface are covered by Xe atoms. The IRAS peak at 2694 cm^{-1} decreased in intensity and/or red shifted by Xe adsorption. The $Xe/D_2O/Rh(111)$ is heated to 77 K in order to desorb Xe adsorbed on the 2D island, Fig. 7.6(c). Xe atoms are adsorbed only on the bare Rh(111) surface, the 2694 cm^{-1} peak do not show change as compared with Fig. 7.6(b). Thus, I conclude that this mode is not the "D-up" species in the 2D islands. Figure 7.6(d) shows IRAS spectrum after flashing to 110 K in order to desorb Xe atoms adsorbed on the bare Rh(111) surface. The peak intensity increased and IRAS spectrum is nearly the same with Fig. 7.6(a). Water molecules at the 2D island edges may strongly interact with Xe atoms adsorbed on the bare Rh(111) surface, thus I conclude that the IRAS peak observed at 2694 cm^{-1} is the stretching mode of free OD at the 2D island edge.

In Fig. 7.5(a), the broad peaks at 2550, 2450, and 2200 cm^{-1} are assigned to the OD stretching vibration of hydrogen–bonded water molecules, because the OD stretching shows a red shift and a peak broadening owing to hydrogen bonds. The IRAS spectrum of crystalline bulk ice exhibits broad peaks from 2600 to 2300 cm^{-1} [Fig. 7.5(b), θ=119].[40] Therefore, the stretching modes of the first water layer, namely around 2550 and 2450 cm^{-1}, are assigned to water molecules hydrogen–bonded to each other in the first layer.

On the other hand, the stretching frequency of 2195 cm^{-1} mode is lower than that of crystalline bulk ice, which indicates an enhanced elongation of the OD bond. Such extremely low–frequency OD stretching bands have been observed for D_2O on Rh(111),[31,33] Pt(111),[41] and Ru(0001).[13] I assign this peak to the OD stretching vibration of D_2O with an OD bond pointing to the Rh(111)

surface, as previously reported for H_2O/Pt(100).[42] This red shift is explained by the weakening and elongation of the internal OD bonds through interaction with the metal substrate.[6] Based on DFT calculation Meng *et al.*[20] reported that the stretching vibration of the D-down species can be characterized by the broad peak at 2200 cm^{-1} of D_2O on Pt(111).[41]

Thus, we conclude that water molecules form D-down domain at low coverage, and the free OD exists at the edge of D-down domain. Based on the LEED results, the D-down domain is the commensurate $(\sqrt{3}\times\sqrt{3})R30°$ structure, in other ward it is flatter than the ice-like zigzag bilayer.

At $\theta \geq 0.36$, a new peak starts to appear at 2723 cm^{-1} in the OD stretching region: while in contrast, the peak intensity of 2694 cm^{-1} decreases [Fig. 7.5(a)]. This new peak exhibits almost the same stretching vibration of free OD at I_h or I_c surface [Fig. 7.5(b), 2724 cm^{-1}].[43] The appearance of this new peak is not explained by the multilayer formation, because the multilayer molecules desorb at lower temperatures than the first layer (see chapter 5). Thus, the ice-like bilayer starts to appear with increasing coverage. By LEED measurements, the compressed hexagon was observed at high coverage region. Therefore, we conclude that the ice-like bilayer is compressed with respect to $\sqrt{3}a_{Rh}$ and ~8° rotated from $[11\bar{2}]$ direction; incommensurate structure. At θ = 1.0, only the peak at 2723 cm^{-1} is observed at free OD region in IRAS. Thus I conclude that the first water layer is mixture of the "D-up" and "D-down" species at high coverage. The coexistence of the D-up and D-down species may be the one which minimizes the long-range dipole-dipole repulsion.

Figure 7.7(a) shows coverage dependence of IRAS spectra at free OD stretching region. Note that two peaks do not shift with increasing coverage, which indicate that the free OD species do not interact with each other. Thus we assume that the peak intensity of these peaks is proportional to their coverage. Figure 7.7(b) shows integrated intensities of these peaks as a function of coverage, the intensities are normalized by a value at θ = 1.0 of 2723 cm^{-1}. With

increasing coverage, the peak at 2694 cm^{-1} grows in intensity and reach maximum at $\theta \sim 0.2$, and then decreased in intensity. The IRAS peak observed at 2694 cm^{-1} is the stretching mode of free OD at the D-down domain island edge. The number of water molecules at the edge of the 2D islands is proportional to θ^{ξ} where $\xi = 1/2$ for disk-like islands and $0.5<\xi<1$ for the 2D islands with jagged circumference. $\xi \sim 0.95$ is estimated by fitting the coverage dependence of 2696 cm^{-1} peak intensity at $\theta \leq 0.2$ and fitted result is shown as dashed curve in Fig. 7.7(b). This indicates that water molecules form very jagged or restricted (anisotropic) D-down islands on the surface.

The D-down model proposed by Ogasawara *et al.*[6] can grow isotropically on the surface, thus islands may show disk-like islands in order to decrease the island edges. Thus, the very jagged or anisotropic islands indicates a different adsorption structure which restrict the isotropic growth like observed for H_2O/Pd(111)[19] and/or small clusters observed for D_2O/Ru(0001)[13]. In order to identify the 2D islands shape, STM measurements should be necessary.

On the other hand, in Fig. 7.7(b), the peak at 2723 cm^{-1} starts to increase in intensity at $\theta \sim 0.2$ and grows linear up to $\theta = 1.0$. The linear growth of the peak intensity of the 2723 cm^{-1} is consistent with our peak assignments that these peaks are derived from the water molecules which have free OD (D-up) inside the 2D islands. The linear increase of the D-up species (2723 cm^{-1}) correlate with the linear decrease of the free OD at the D-down domains (2694 cm^{-1}), this result indicates that the D-up domains start to grow from the edge of D-down domains and occupy among the D-down domains.

I shortly summarize the results at submonolayer region (Fig. 7.8). At the initial stage, water molecules form the commensurate $(\sqrt{3}x\sqrt{3})R30°$structure. This is flatter than ice-like bilayer, and consists of the D-down species. Free OD at the D-down island edge shows the stretching mode at 2696 cm^{-1} in IRAS. Based on the coverage dependence of the peak intensity (2696 cm^{-1}), D-down

islands may have jagged edges or anisotropuc island shape. With increasing coverage, the ice-like bilayer (D-up) grows and show the incommensurate. At nearly the saturation coverage, the ice-like bilayer is ~9 % compressed from the commensurate ($\sqrt{3}x\sqrt{3}$)*R*30°structure, which is ~5 % compression with respect to ice I_h. At saturation coverage, the first water layer consists of the ice-like bilayer (D-up) and flat (D-down) domains.

Taking into account the above results, I assigned the DOD bending (δ_{DOD}) and librational modes as follows. At low coverage region, two peaks at 1187 and 1172 cm^{-1} are observed in the δ_{DOD} region. At the initial stage of first layer growth, water molecules form the D-down islands, where two kinds of water species exist: water molecule which bonds to the metal atom via their oxygen lone pair and has OD bond pointing to the substrate (D-down species). Assuming that the frequency of the bending mode decreases from its gas–phase value (1178 cm^{-1}) as the extent of charge transfer to the substrate metal increases,[1] the peak at 1172 cm^{-1} is assigned to water molecules, which are bonded to metal atoms via their oxygen lone pair. In addition, taking into consideration the fact that the intermolecular hydrogen bond causes a blue shift in δ_{DOD},[1] the peak at 1187 cm^{-1} is assigned to the D-down species. With increasing coverage, a new peak appears at 1199 cm^{-1} and increase in intensity, where shoulder peaks at 1206 and 1230 cm^{-1} are observed.

In the D_2O librational region, two peaks are observed at 657 and 610 cm^{-1} at low coverage. With increasing coverage, these peaks grow in intensity. Thus these modes are not derived from the edge species: water molecules inside the D-down islands. In addition, new peaks start to appear at 706 and 520 cm^{-1}. At saturation coverage, four peaks are observed.

Figure 7.9 shows top and side views of three adsorption geometries and the dipole-active (i.e. the totally symmetric) modes at the different geometries. Figure 7.9(a) shows the water molecule bonding to the substrate via their oxygen lone pair. This water molecule has three hydrogen bonds between water

molecules; accepting one and donating two hydrogen bonds. Thus, two OD bonds are identical. Here note that two kinds of water molecule of this geometry exist on the surface: in the D-up and D-down domains. Figure 7.9(b) and (c) shows the D-down and D-up species. In these configurations, two OD bonds are not identical. These three geometries results in one dipole-active hindered rotation (libration) mode, respectively.

At low coverage, two peaks observed at 657 and 610 cm^{-1} are assigned as follows. Because the librational frequency decreases as the strength and tetrahedrality of the hydrogen bond decreases,[44] the peak observed at 657 cm^{-1} is assigned as out of plane hindered rotation of water molecule bonding to the substrate via their oxygen lone pair in the D-down islands. Thus, the 610 cm^{-1} peak is assigned as in plane hindered rotation of D-down species. At high coverage region, two peaks start to appear at 706 and 520 cm^{-1}. Based on the above discussions, these two peaks are assigned as out of plane hindered rotation of water molecule bonding to the substrate via their oxygen lone pair in the D-up domain and in plane hindered rotation of D-up species, respectively. Yamada et al. reported that the surface hindered rotational modes of single–crystalline ice grown on Pd(111) appeared at 500 cm^{-1}.[45] The peak at 520 cm^{-1} observed in the present experiment are in good agreement with the reported surface hindered rotational mode.

Here, note that on Pt(111) the first water layer at the saturation coverage shows the $(\sqrt{39}\times\sqrt{39})R16.1°$ phase, in which water molecules are laterally compressed by 3.3 % compared to the bulk ice I_h.[15,16] From recent calculations, one key feature of the $(\sqrt{39}\times\sqrt{39})R16.1°$ phase is that 9 % of water molecules are ionised as H_3O^+ and OH^-, due to both lateral compression of the water layer and its interaction with the substrate.[17] However, in the present experiment, no IRAS peak was observed at the 800 ~ 850 cm^{-1} region, which is characteristic of D_3O^+ (isotopic shifted)[46]. Thus, I conclude that the first D_2O layer molecularly wets the Rh(111) surface.

7.3.1.C Water coadsorption with oxygen

I investigated the effect of preadsorbed oxygen on the adsorbed state of water on Rh(111). Figure 7.10 shows the IRAS spectra in the librational region. Oxygen molecules were adsorbed at 20 K, and then annealed to 300 K to dissociate the molecule into oxygen atoms [Fig. 7.10(a)].[31] The coverage of oxygen atoms was about 0.06 ML. Figure 7.10(a) shows only a small peak at 516 cm^{-1}, which is assigned to the stretching vibration of Rh–O.[35] Water molecules were dosed on O/Rh(111) at 20 K, followed by annealing at 155 K for 60 s [Fig. 7.10(b)]. This treatment induces a new peak at 771 cm^{-1}, which is assigned to the bending mode of a hydroxyl species (Rh–OD).[31] Since this peak is not observed in the pure water layer (Fig. 7.5), we conclude that water molecules are not dissociated on the Rh(111) "clean" surface. In addition, the TPD spectrum of this layer is shown in the inset of Fig. 6.3(a). The desorption peak at 202 K is a feature for the desorption from the OD+D_2O mixed layer.

7.3.1.D Titration of D-up and D-down species on Rh(111)

In the previous section, I elucidated that the first water layer on Rh(111) consists of a mixture of the D-up and D-down species. In this section, I estimate the fractional coverage of the D-up and D-down species at θ=1.0.

In order to estimate the coverage of the D-up and D-down species, I exposed the D_2O layer to H_2O molecules at 20 K. I expected that the H_2O molecules interact with free OD via its oxygen lone pair; and the decay kinetics of free OD as a function of dosed H_2O coverage $\theta(H_2O)$ would give the coverage of the D-up species.

$\theta(H_2O)$ was estimated as follows. I measured the coverage as a function of H_2O exposure on Rh(111), where H_2O was adsorbed at 135 K. Based on a coverage increment of multilayer as a function of exposure, $\theta(H_2O)$ was

determined. Note that I assumed the sticking probability to be unity between H_2O on the saturated H_2O/Rh(111) at 135 K and H_2O on the saturated D_2O/Rh(111) at 20 K.

Figure 7.11 shows the IRAS spectra of OH and OD stretching vibrations as a function of adsorbed H_2O coverage. With increasing H_2O exposure, the intensity of the free OD stretching vibration at 2723 cm^{-1} decreases. In addition, new peaks appear at 3719, 3698, 3430 and 3200 cm^{-1}, respectively, and their intensities increase with increasing H_2O exposure.

These new peaks at 3719 and 3698 cm^{-1} are derived from the OH stretching mode of free OH groups with 2–coordinated and 3–coordinated surface H_2O molecules, respectively.[39] It should be noted that neither proton exchange nor interlayer mixing[37] between the first D_2O layer and post–dosed H_2O molecules was observed during the adsorption process at 20 K. Proton exchange and interlayer mixing should provide a bending mode of HDO (1370 cm^{-1} for the first layer)[31] and a stretching mode of 2–coordinated free OD (2750 cm^{-1}) in IRAS,[39] respectively. However, I did not observe them. In addition, the new peaks at 3430 and 3200 cm^{-1} may be derived from a hydrogen donor in the form of 2– or 3–coordinated and/or 4–coordinated H_2O molecules.[47]

At the early stage of H_2O adsorption [$\theta(H_2O) \leq 0.16$], 2–coordinated H_2O molecules are preferential species on the D_2O first layer, judging from the peak intensity. With increasing H_2O coverage, IRAS peaks of 3–coordinated and 4–coordinated H_2O molecules start to appear at $\theta(H_2O) \geq 0.21$. Here, I propose the following model concerning H_2O adsorption on the D_2O layer. When a single H_2O molecule adsorbs on the D_2O first layer, H_2O bonds to the free OD via its oxygen lone pair, and may be observed between 3719 and 3755 cm^{-1} (asymmetric stretching vibration of gas phase water molecule). However, a 1–coordinated water molecule is not observed. Since this species is not stable[47] and mobile on the D_2O layer, they migrate until they collide with the other migrating H_2O molecules, and finally form a stable cyclic hexagonal ring. A

model of this ring structure is shown in Fig. 7.12. Note that three H_2O molecules are involved in this structure and they are all 2–coordinated. Therefore, this model is consistent with the observed results, in which 2–coordinated H_2O species are dominant at the early stage of H_2O adsorption [$\theta(H_2O)\leq 0.16$] at 20 K. In this model, two free OD bonds are bonded to three H_2O molecules.

Figure 7.13 shows the intensity of the free OD stretching mode at 2723 cm^{-1} as a function of $\theta(H_2O)$. In this figure, the peak intensity is normalized by the initial peak intensity (before the H_2O adsorption). With increasing H_2O coverage, the peak intensity of free OD rapidly decreases. In the case of a hit–and–stick model on an ice surface,[48] a simulated curve (dot–dashed curve in Fig. 7.13) does not support the observed results at all. This also indicates surface diffusion of incoming H_2O molecules; H_2O molecules migrate on the D_2O layer until they form a cyclic hexagonal ring. Because of the recent result, where a fully coordinated water monolayer on Pt(111) results in a hydrophobic surface on which water diffusion is facile,[24] this assumption may be valid.

In this migration–clustering model on the D_2O layer, we can estimate the maximum coverage of the D-up species. From the adsorption kinetics based on this model, we apply a linear decay at $\theta(H_2O)\leq 0.16$ (the solid line in Fig. 7.13). A gradient of this line is estimated to be –3.0. This value should be equal to $-2/[3\times\theta(\text{free OD})]$; θ(free OD) is the fractional coverage of free OD sites. By the same token, θ(free OD) is estimated to be 0.22. Since the first water layer on Rh(111) consists of a mixture of the D-up and D-down species, the maximum coverage of the D-up domain and the minimum coverage of the D-down domain is estimated to be $0.22\times 2=0.44$ and $1-0.44=0.56$ at the saturation coverage (θ=1.0), respectively. Thus the amount of D-down species is 1.3 times larger than that of the D-up species on Rh(111) (θ=1.0).

7.3.1.E Wetting or dewetting of water molecules on Rh(111)

Feibelman has proposed that water molecules on Rh(111) must be dissociated by impurity atoms on the surface in order to explain the wetting layer, because the calculated heat of adsorption disfavors intact-molecule wetting layers, compared with the formation of 3D ice mounds.[34] In addition, he has proposed that entropy effects hardly contribute to the free energy, and adsorption energies at T=0 K dominate in the free energy between wetting and dewetting, even at 150 K.[49] In fact, experimentally, the wetting–dewetting transition was reported for H_2O on Ag(110) at 133.5 K[50] and D_2O on Pd(111) at 130 K.[19]

In the present study, we clearly reveal that water molecules wet the Rh(111) surface molecularly as previously reported.[29-33] From the TPD results, water molecules wet the Rh(111) surface intact at $\theta \leq 0.6$ simply because of the adsorption energy (see chapter 6). Since this result contradicts the theoretical study, either DFT is simply inadequate to calculate the energetics to the required accuracy and dispersion forces must be included,[51] or the structure of the wetting layer differs from the bilayer assumed previously.[3]

On the other hand, from an energetic point of view, water molecules could not wet but only dewet the Rh(111) surface at $\theta \geq 0.6$. To examine the wetting–dewetting transition for D_2O on Rh(111), the first water layer at $\theta=1.0$ was annealed at 130~135 K (below the temperature of multilayer desorption) for 1200 s. If the wetting–dewetting transition occurs, a bare Rh(111) surface must be partly exposed to vacuum. Then, I exposed this annealed water layer to CO molecules. However, no stretching vibration of CO on Rh(111) was observed by IRAS; thus, there was no bare Rh(111) surface after this annealing. Therefore, I conclude that no wetting–dewetting transition occurs in this experimental condition for D_2O on Rh(111) at $\theta=1.0$. Thus, the dewetting on Rh(111) may be a kinetically hindered process. Entropy effects may also contribute to the free energy. In fact, water molecules exist as the D-up and D-down configurations

with a slight energy difference (0.3 kJ/mol), which could increase entropy over the entire system.

7.3.2 Multilayer growth of water on the Rh(111) surface

Based on the previous section, we investigated a crystalline ice growth on the first water layer. The first water layer on the Rh(111) surface is the mixture of D-up and D-down species. As explained above, the D-up species has one free OD pointing to a vacuum (hydrophilic) whereas a fully coordinated water layer by D-down species results in a hydrophobic surface. Therefore, the first water layer on the Rh(111) surface has hydrophilic (D-up) and hydrophobic (D-down) domains.

Kimmel et al. investigated the morphology of thin water films grown on the Pt(111) and Pd(111) surfaces using a Kr TPD.[24,25] The van der Waals interaction of a rare gas atom with a metal surface is a sensitive function of the distance between them. As a result, the TPD spectra of multilayers of rare gas atoms adsorbed on a metal surface typically have a series of peaks at ascending temperature due to desorption of adlayers successively closer to the substrate. Thus the TPD spectra can be used to assess the height of a desorbing atom above a metal surface. This same approach can also be used to determine the height distribution of a thin water film grown on the Rh(111) substrate.

Figure 7.14 shows Xe TPD spectra adsorbed on D_2O/Rh(111) as a function of water coverage at submonolayer region. Water molecules were adsorbed on Rh(111) at 150 K, and then Xe atoms (~1 ML) were adsorbed at 20 K followed by TPD measurement. Peaks around 100 K are assigned to a desorption of Xe atoms adsorbed on the bare Rh(111) surface. At θ = 0.14, this peak decreased in intensity and leading edge shifts to lower temperature. In addition, new peaks appear at 72 K and small peak is observed at 67 K. In this

study, I labeled these peaks observed at 72 and 67 K as α_1 and α_2, respectively. On the clean surface, these peaks are not observed, thus these peaks can be assigned to desorption of Xe atoms adsorbed on the 2D water islands. Based on the results of previous section, water molecules form the commensurate $(\sqrt{3}x\sqrt{3})R30°$structure with D-down configuration at low coverage region. In Xe TPD, the α_1 peak is dominant compared with the α_2 peak at θ = 0.14. Thus, the α_1 peak is assigned to desorption of Xe atoms adsorbed on the D-down domains.

With increasing water coverage, α_1 peak increased in intensity and shift to higher temperature. Subsequently, the α_2 peak increased in intensity and shift to higher temperature. Based on the previous section, the ice-like bilayer grows at high coverage region. Thus, the α_2 peak is assigned to desorption of Xe atoms adsorbed on the D-up domains.

Therefore, I can titrate the D-up and D-down domains using Xe TPD. At saturation coverage, a ratio of the integrated peak intensity of α_1 with respect to α_2 is 1.2. Assuming a linear heating rate in this desorption region and a same adsorption structure of Xe on D-up and D-down domains, it is consistent with the previous titration experiment (section 7.3.1.D) where the amount of D-down species is 1.3 times larger than that of the D-up species.

Figure 7.15(a) shows TPD spectra of Xe adsorbed on D_2O/Rh(111) as a function of water coverage at multilayer region. D_2O was adsorbed at 135 ~ 140 K followed by Xe adsorption at 20 K. Multilayer or second layer Xe was desorbed before the TPD measurements, thus only the Xe desorption adsorbed on the first water layer (α_1 and α_2 peaks) are observed. With increasing the water coverage, desorption peaks decreased in intensity where α_1 peak firstly decreases. This result means that adsorption sites of Xe on the D-down domains firstly decrease by water adsorption. Thus, water multilayer starts to grow on the D-down domains. Here, multilayer formation may not cause structural change of the D-down domains, because the stretching mode of D-down species (2195 cm^{-1})

at θ = 1.4 does not show any changes compared with that at θ = 1.0 as shown in Fig. 7.5(b).

Figure 7.15(b) shows the water coverage dependence of the integrated peak intensity ($\alpha_1 + \alpha_2$), which is identical to a fractional coverage of the bare first water layer. With increasing water coverage, the fractional coverage of the bare first water layer decreased, but the crystalline water films do not fully wet the first water layer up to θ ~ 100. Therefore, three-dimensional water islands are formed on the first water layer.

In the previous section, I conclude that the D-up domain is ~5% compressed compared with ice I_h. If the water multilayer grows epitaxially on the D-up domain, crystalline ice becomes unstable compared with ice I_h because of strain (compression) energy. In addition, epitaxial growth of crystalline ice on the D-up domain may results in a net polar ordered ice which has lower entropy than ice *I* because hydrogen atoms are randomly situated in ice *I*. Therefore, water molecules prefer to aggregate each other on the D-down domain in order to form 3D crystalline (ice I_h or I_c) grains with no hydrogen bonds between the first water layer and multilayer. In the previous section, water molecules form vertical hexagonal ring on the D-up domain at 20 K (Fig. 7.12). This small cluster may not be stable at 140 K, thus water molecules migrate on the first water layer to form large crystalline 3D grains. Therefore, the vertical hexagonal ring may be a precursor in order to form the three-dimensional ice grains on the first water layer.

7.4 Discussions

The Xe adsorption experiments described above show that water adsorption at 135 K formed 3D crystalline islands on the first water layer. This behavior has

been observed previously on other metal substrate such as Pt(111)[24,25], Pd(111)[25], and Ru(0001)[26,27]. In these studies, the structures of the first water layer are considered as H-down model, where a fully coordinated water layer by H-down species results in a hydrophobic surface.

Based on the above idea, H-up species may result in a hydrophilic surface, because one free OH can donate a hydrogen bond. However, water multilayer start to grow on the D-down domains and do not wet the first water layer on the Rh(111) surface, where the D-up and D-down species coexists. Thus, D-up species do not result in a hydrophilic surface. This indicates that the hydrophobic and hydrophilic properties of the first water layer are not simply controlled by the water arrangement; H-up or H-down.

In previous studies, a microscopic structure at the interface between first layer and multilayer is rarely obtained. Su *et al.* studied the growth of water multilayer on Pt(111) at 120~137 K using SFG (second harmonic generation).[52] They reported that hydrogen bond network is not random (i.e., isotropic) but exhibits a ferroelectric order (the term is used here to describe a net polar ordering of water molecules in the ice film). The observation of a SFG peak characteristic of a free OH stretch at $\theta = 1.2$ and above raises the possibility that the structure of the first water layer on Pt(111) could be modified when the second layer grows on top, because the first water layer arranges as H-down on this surface.

On the other hand, in this study, it is elucidated that the D-down species do not reorient to accommodate formation of a crystalline ice when the second layer start to grow on the D-down domain on Rh(111). This result is clear evidence for a hydrophobic interaction; hydrogen bonding within the multilayer is favored compared to bonding to the first water layer.

In addition, it is elucidated that a lattice matching between substrate and the basal plane of ice I_h do not ensure an epitaxial growth of ice I_h, where the D-down domain adopts commensurate structure with the Rh(111) surface which

has small lattice mismatch of ~3%.

Previous studies are summarized as shown in Fig. 7.16, in which the reported growth mechanisms of water ice are lined up in the order of periodic tables of the substrate metal atom. This order may correlates with the adsorption energy (E_{ad}) of water molecules because the dominant interaction of water molecule with metal substrate may be the electron donation from water $1b_1$ orbital (lone pair) to the substrate *d*-bands.

Water molecules weakly interact with the noble metal substrates, because of weak hybridization of water $1b_1$ with metal *sp* bands. In these cases, water-water interaction (hydrogen bonding) governs water-metal interaction, thus water molecules do not wet the substrates, namely hydrophobic metal substrate.

On the other hand, for transition metal substrates, water molecules interact more strongly with surfaces. On the Ni(111) surface, the first water layer shows the high-order commensurate 2D structure. When a second-layer is formed, water film reconstructs to an incommensurate crystalline ice. In addition, water film grows layer-by-layer on the Ni(111) surface. In other words, this surface results in hydrophilic metal surface.

In the case of the Pt(111), Pd(111), Rh(111), and Ru(0001) surfaces, the first water layer wet these surfaces (hydrophilic metal surface), however water ice nucleate on these first water layers as 3D islands. In this study for Rh(111), 3D islands grows on the D-down domains where D-down species does not reorient in order to accommodate formation of a crystalline ice. This behavior results in the hydrophobic first water layer. Thus, I think that not the water arrangement but the capability of reorientation (reconstruction) of water molecules in the first water layer is crucial in order to understand the film growth mechanism on metal substrates.

7.5 Conclusion

The adsorption states and growth process of the first water (D_2O) layer and multilayer on Rh(111) were investigated using IRAS, TPD, and SPA–LEED. At the initial stage, water molecules form the commensurate ($\sqrt{3}$x$\sqrt{3}$)*R*30°structure. This is flatter than the ice-like bilayer, and consists of the D-down species. Free OD at the D-down domain edge shows the stretching mode at 2696 cm^{-1} in IRAS. Based on the coverage dependence of the peak intensity (2696 cm^{-1}), 2D islands may have jagged circumference or anisotropic island shape. With increasing coverage, the ice-like bilayer grows and shows the incommensurate structure. At nearly the saturation coverage, the ice-like bilayer is ~9% compressed from the commensurate ($\sqrt{3}$x$\sqrt{3}$)*R*30° structure, which is ~5% compression with respect to ice I_h. At saturation coverage, the first water layer consists of the ice-like bilayer (D-up) and flat (D-down) domains, where the D-up and D-down domains occupy 44 % and 56 % of the first water layer respectively. Further adsorption of water molecules form 3D ice crystallites on the D-down domains where the D-down species do not reorient to accommodate formation of a crystalline ice.

Figures and table

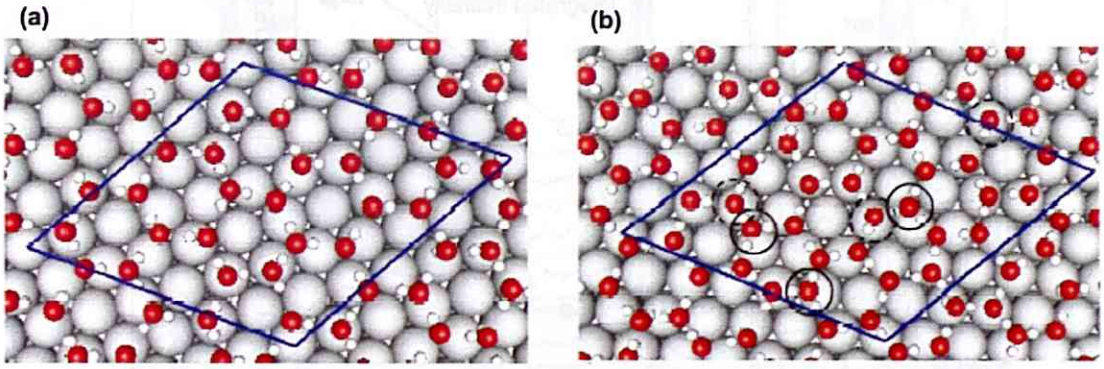

Fig. 7. 1. Proposed models of (a) the (√37x√37)R25.3° (H-down) and (b) the (√39x√39)R16.1° (H-down).[17]

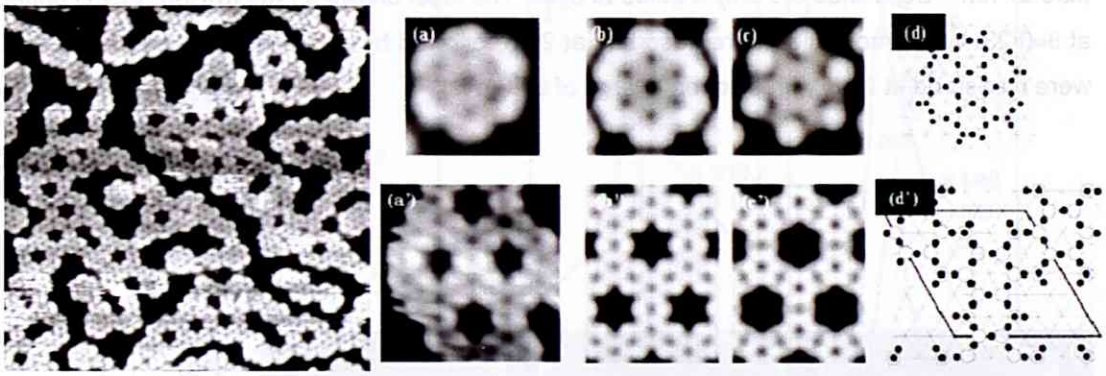

Fig. 7. 2. Experimental and simulated STM images of D_2O clusters on Pd(111). Left: STM image of D_2O clusters on Pd(111) at 100 K. Right: (a) Experimental STM image of a rosette structure made of seven hexagons. (b and c) STM topographic image simulations for two different DFT-optimized models of the rosette structure. In panel b, the edge water molecules have a H-down configuration. In panel c, alternating molecules are dissociated to OH (a similar simulated image was obtained from an H-up configuration). (d) DFT optimized structure of panel b. White circles are O atoms, and dark circles are H-atoms. Dirk circles inside white circles are dangling H-atoms below the O-atoms (H-down). Panels a'-d' show the results for a larger structure. Again, the STM images can be reproduced only with edge molecules with dangling H-atoms toward the surface.[19]

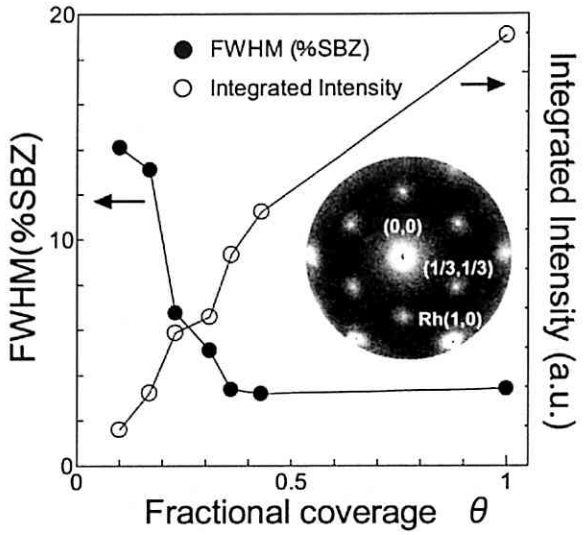

Fig. 7. 3. FWHM and integrated intensity of a (1/3,1/3) LEED spot as a function of water coverage. 100 %SBZ corresponds to the normal spot distance of the Rh(111) surface, k = $2\pi/0.27$ nm^{-1}. Solid lines are only a guide to eyes. The inset shows a ($\sqrt{3}\times\sqrt{3}$)R30° LEED pattern at θ=0.23. Water molecules were adsorbed at 20 K followed by annealing at 145 K. All the data were measured at 20 K with electron energy of 60.6 eV.

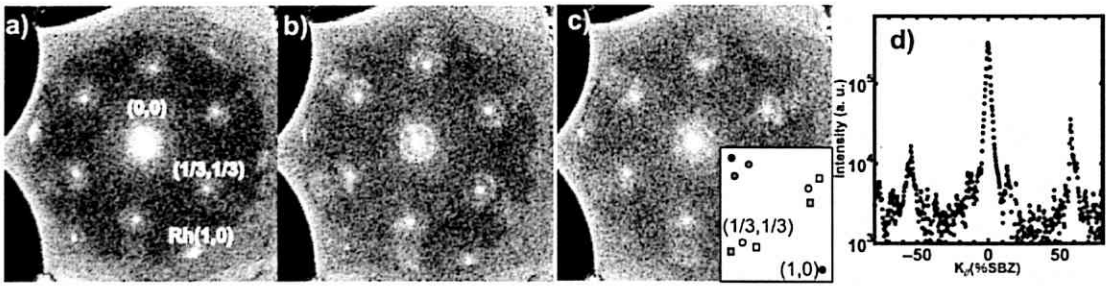

Fig. 7. 4. LEED patterns for D_2O adsorbed on Rh(111) at 135 K observed with incidental electron energy of 60 eV at 85 K. (a) θ = 0.25, (b) θ = 0.56, (c) θ = 0.89. The insets of panel (c) are illustrated schematically of diffraction pattern. (d) One-dimensional cut along $[1\bar{1}2]$ of panel (c). 100 %SBZ corresponds to the normal spot distance of the Rh(111) surface, k = $2\pi/0.27$ nm^{-1}.

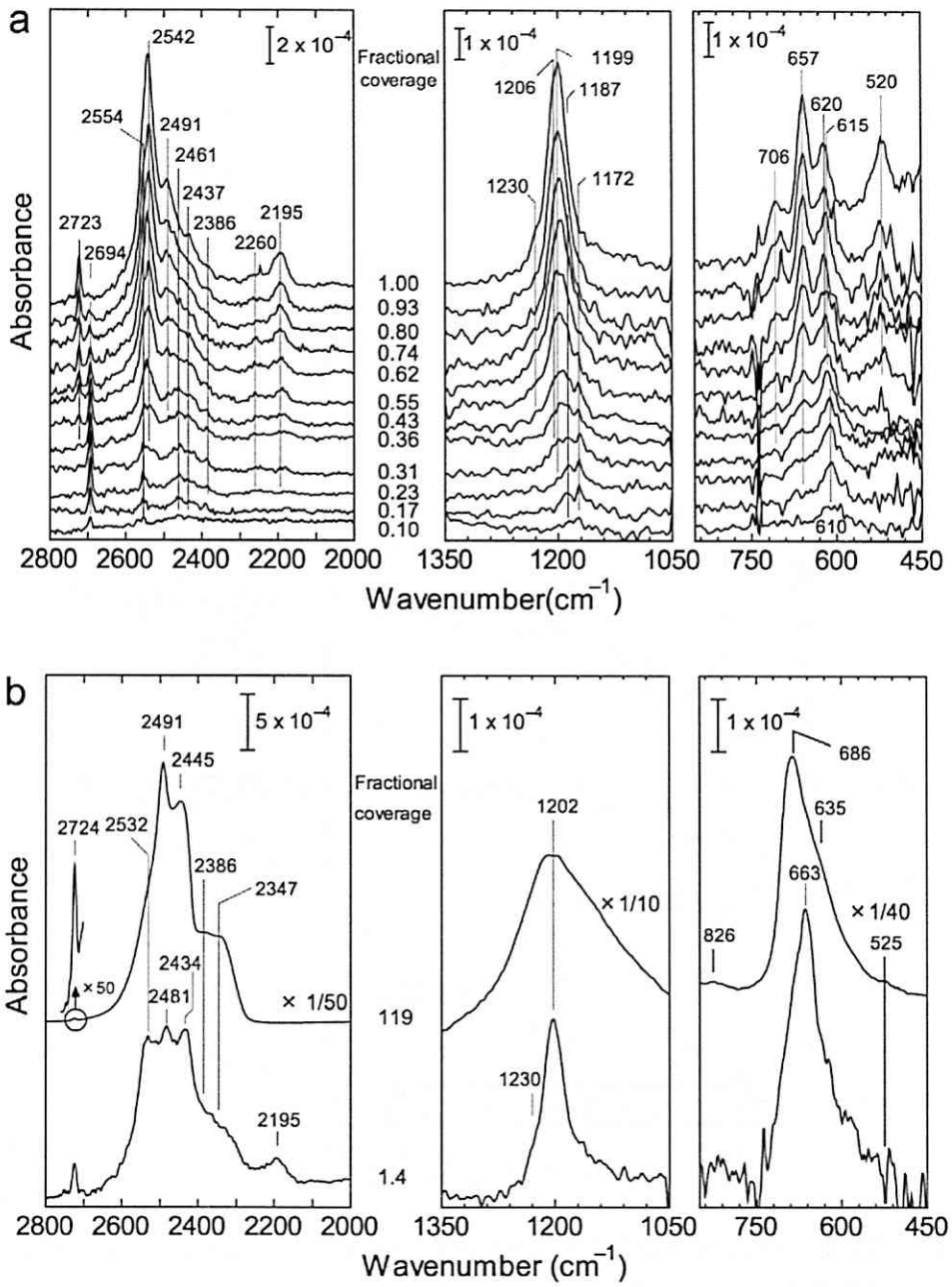

Fig. 7. 5. (a) IRAS spectra of D_2O on Rh(111) as a function of coverage (the submonolayer region). Water molecules were adsorbed at 20 K followed by annealing at 145 K. All the spectra were measured at 20 K with 4 cm^{-1} resolution and 500 scans by the Si:B detector. (b) IRAS spectra of D_2O on Rh(111) as a function of coverage (the multilayer region). All the spectra were measured at 20 K with 4 cm^{-1} resolution and 500 scans by the Si:B detector. The multilayer ice of θ=1.4 and θ=119 was made by epitaxial growth and annealing an ASW multilayer at 165 K to crystallize, respectively.

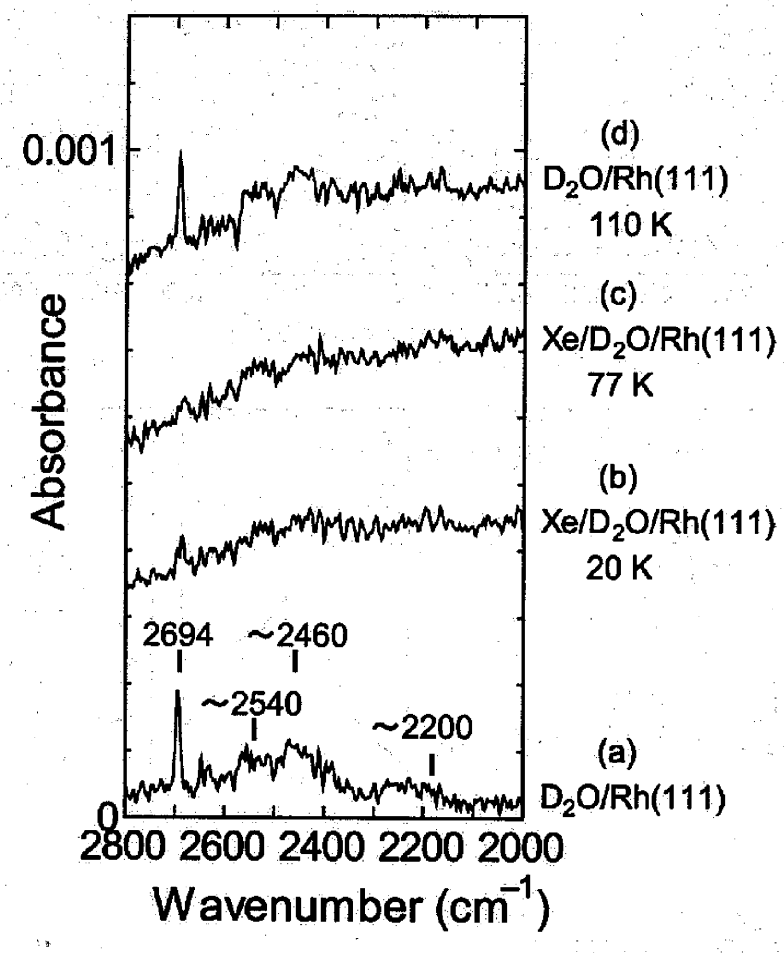

Fig. 7. 6. IRAS spectra of $Xe/D_2O/Rh(111)$ as a function of Xe observed at 20 K. (a) IRAS spectrum of $D_2O/Rh(111)$ at θ=0.14, where water molecules were adsorbed at 155 K. (b) IRAS spectrum of $Xe/D_2O/Rh(111)$, where water layer (θ =0.14) are exposed to Xe at 20 K. (c) The $Xe/D_2O/Rh(111)$ is flashed to 77 K. (d) IRAS spectrum after flashing to 110 K. All the spectra were measured at 20 K with 4 cm^{-1} resolution and 500 scans by the MCT detector.

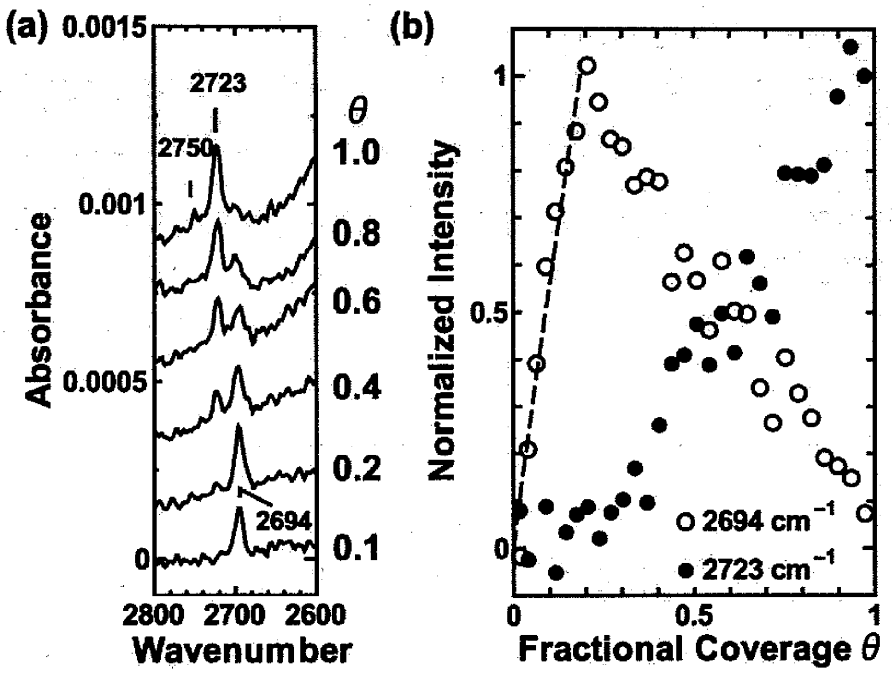

Fig. 7. 7. (a) Coverage dependence of IRAS spectra at free OD stretching modes region. Water molecules were adsorbed with an average flux of ~0.0003 (fractional coverage)/s at 135 K followed by IRAS measurement at 135 K. (b) Coverage dependence of IRAS peak intensities. Fitted result is shown as dashed curve.

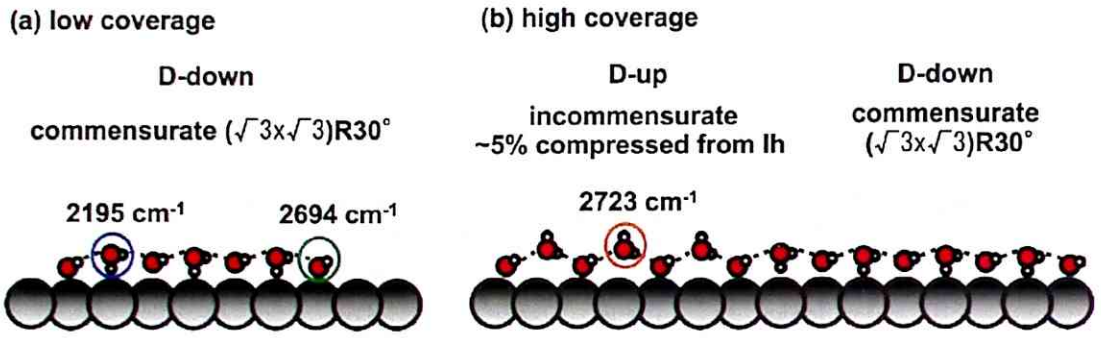

Fig. 7. 8. A schematic illustration of the first water layer at (a) low coverage and (b) high coverage region, respectively.

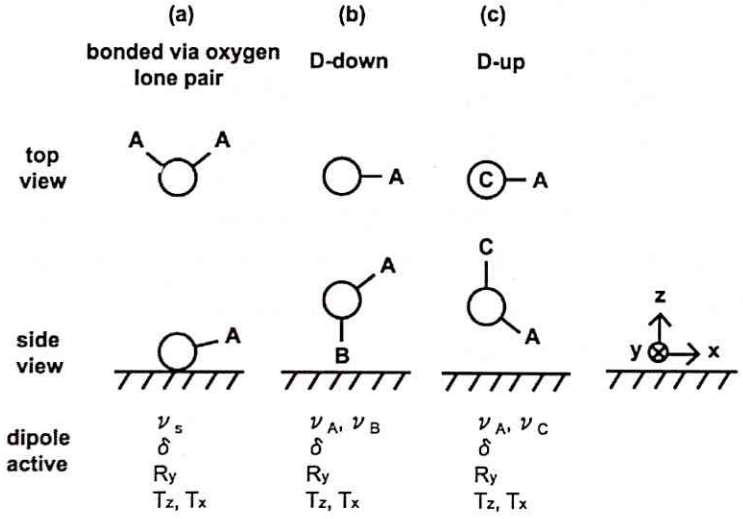

Fig. 7. 9. Top and side views of three different adsorption geometries and the dipole-active (i.e. totally symmetric) modes at the different geometries. The intramolecular modes are labeled δ (D-O-D bend) and ν (O-D stretch). The hindered rotation and hindered translations are labeled R and T with respect to axes fixed to the substrate, respectively. (a) Water molecule bonding to the substrate via their oxygen lone pair. (b) D-down (c) D-up species.

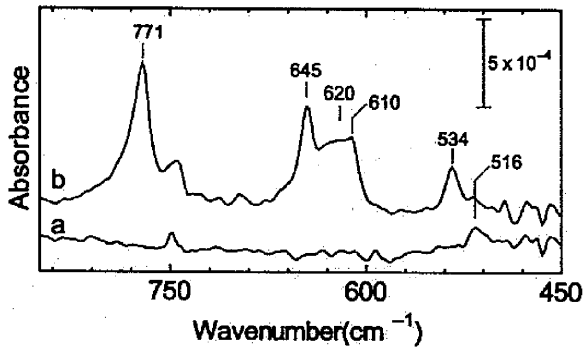

Fig. 7. 10. IRAS spectra (850 to 450 cm^{-1}) of (a) O/Rh(111) (~0.06 ML), (b) D_2O/O/Rh(111). (a) Oxygen molecules were adsorbed at 20 K on Rh(111) followed by annealing to 300 K. The coverage of oxygen atoms is about 0.06 ML. (b) Water molecules were dosed on O/Rh(111) at 20 K, followed by annealing at 155 K for 60 s. Both spectra were measured at 20 K with 4 cm^{-1} resolution and 500 scans by the Si:B detector. An unwanted signal at 750 cm^{-1} is due to noise.

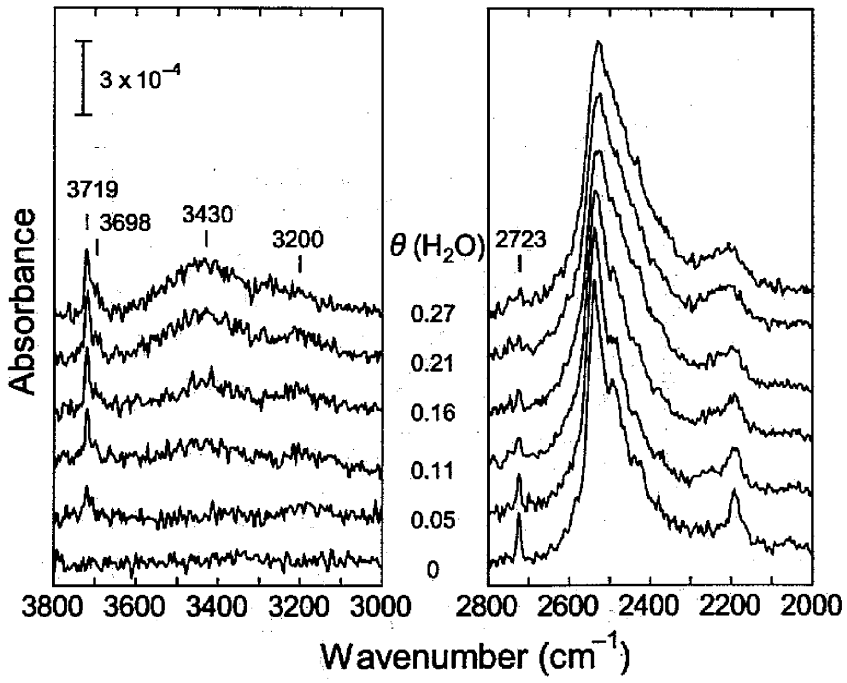

Fig. 7. 11. IRAS spectra of D_2O at θ=1.0 on Rh(111) as a function of adsorbed H_2O coverage. The D_2O layer (θ=1.0) was made by annealing an ASW film at 145 K, and then it was exposed to H_2O at 20 K. All the spectra were measured at 20 K with 4 cm^{-1} resolution and 500 scans by the MCT detector.

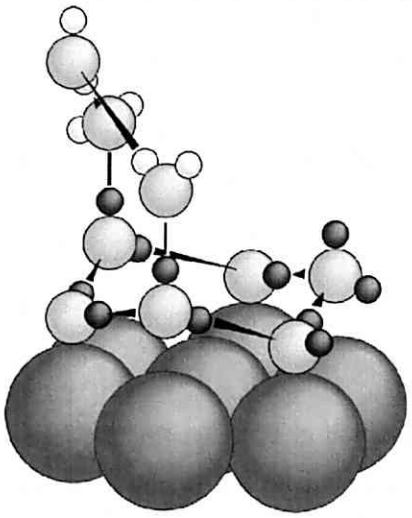

Fig. 7. 12. A schematic structural model for H_2O adsorption on the D-up domain. Gray and white small circles represent deuterium and hydrogen atoms, respectively. Bold lines represent hydrogen bonds.

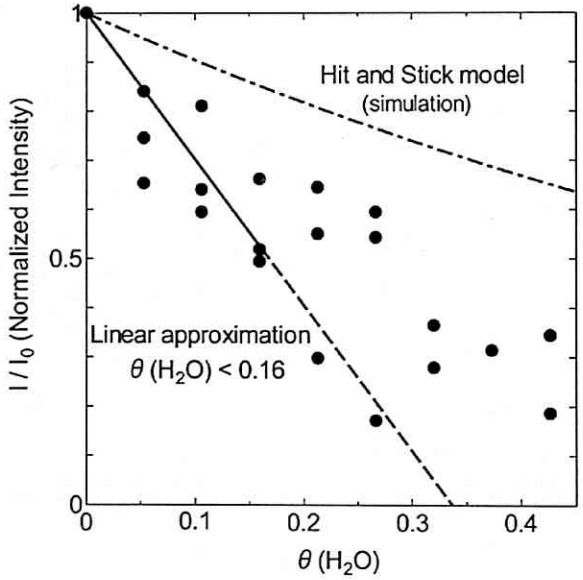

Fig. 7. 13. The intensity of 2723 cm^{-1} peak normalized by the initial peak intensity as a function of H_2O coverage. The dot-dashed curve is a simulated decay based on a hit and stick model. The solid line is fitted by a least squares approximation at $\theta(H_2O) \leq 0.16$.

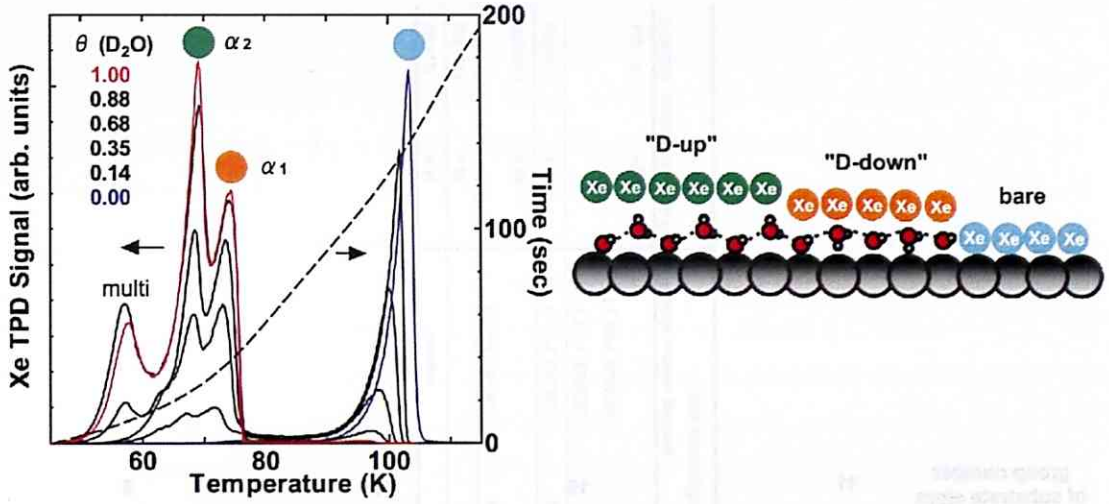

Fig. 7. 14. Xe TPD spectra for ~1 ML Xe deposited on the D_2O/Rh(111) surface. Time at each temperature is illustrated as dotted curve.

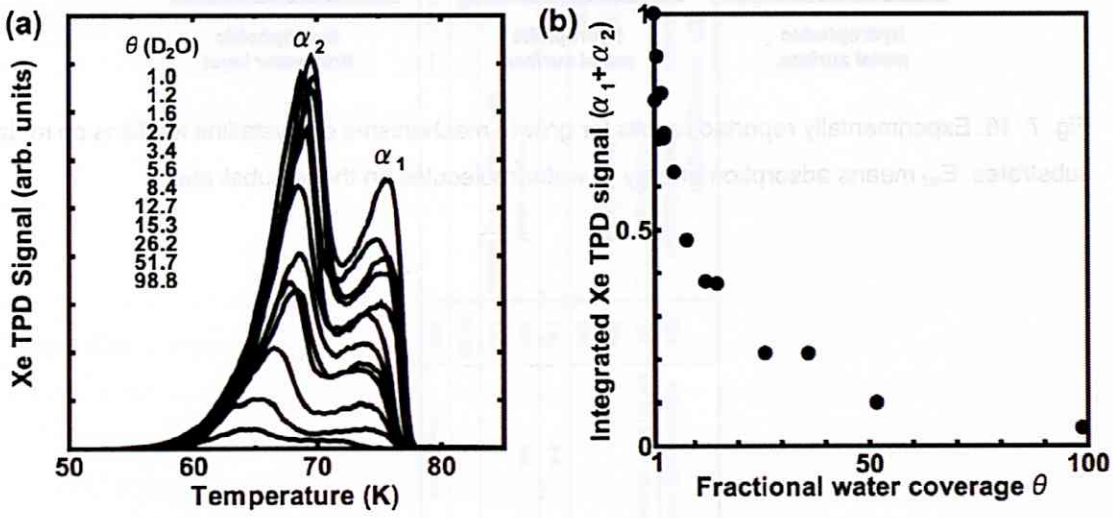

Fig. 7. 15. (a) Xe TPD spectra deposited on the multilayer D_2O/Rh(111) surface. Multilayer and/or second layer Xe were desorbed before TPD experiments. (b) Fractional coverage of Xe, (α_1 + α_2), adsorbed on the first water layer as a function of water coverage.

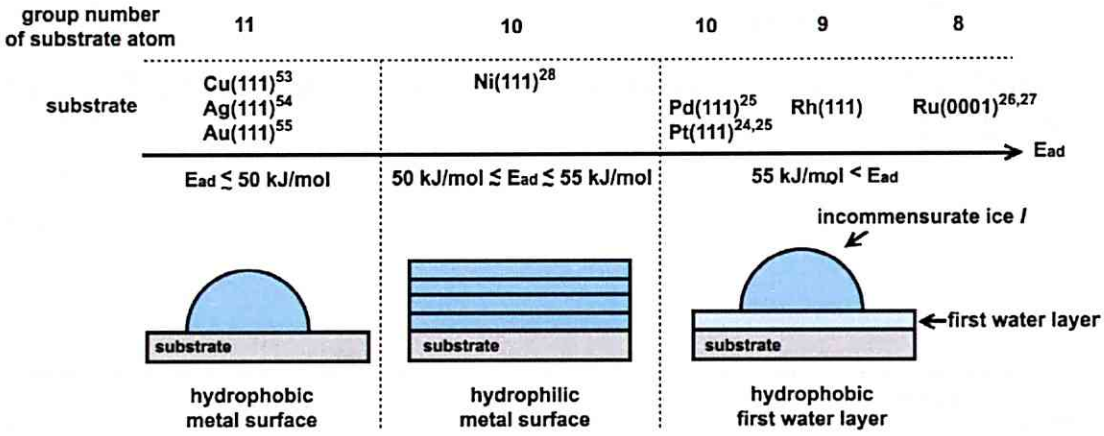

Fig. 7. 16. Experimentally reported results for growth mechanisms of crystalline ice films on metal substrates. E_{ad} means adsorption energy of water molecules on these substrates.

substrate	lattice parameter (Å)	low coverage region		high coverage region		Ref.	Multilayer growth mode	Ref.
		long-range ordered structure	water configuration	long-range ordered structure	water configuration			
Pt(111)	4.80	-	-	-	H-down model	[9]	S-K (2D layer + 3D islands)	[24,25]
		($\sqrt{37}$x$\sqrt{37}$)R25°	H-down model	($\sqrt{39}$x$\sqrt{39}$)R16°	H-down model	[15]		
		($\sqrt{37}$x$\sqrt{37}$)R25°	-	($\sqrt{39}$x$\sqrt{39}$)R16°	-	[10]		
Pd(111)	4.76	($\sqrt{3}$x$\sqrt{3}$)R30°	flat + H-down species	-	-	[16]	S-K	[26]
Ru(0001)	4.69	-	H-down model	-	H-down model	[13]	S-K	[27]
		($\sqrt{3}$x$\sqrt{3}$)R30°	flat + H-down species	disorder	flat + H-down + H up species	[14]		
Rh(111)	4.86	-	-	($\sqrt{3}$x$\sqrt{3}$)R30°	-	[29-32]	-	
Ni(111)	4.31	disorder	-	(2$\sqrt{7}$x2$\sqrt{7}$)R19°	-	[28]	Layer-by-layer	[28]

Table 7. 1. Recent experimental results of the first water layer and multilayer growth mechanism on transition metal surfaces. Lattice parameters are represented in √3a, where a is the lattice constant of the surface.

References

1. P. A. Thiel and T. E. Madey, Surf. Sci. Rep. **7**, 211 (1987).
2. M. A. Henderson, Surf. Sci. Rep. **46**, 1 (2002).
3. D. L. Doering and T. E. Madey, Surf. Sci. **123**, 305 (1982).
4. G. Held and D. Menzel, Surf. Sci. **316**, 92 (1994).
5. S. R. Puisto, T. J. Lerotholi, G. Held, and D. Menzel, Surf. Rev. Lett. **10**, 487 (2003).
6. H. Ogasawara, B. Brena, D. Nordlund, M. Nyberg, A. Pelmenschikov, L. G. M. Pettersson, and A. Nilsson, Phys. Rev. Lett. **89**, 276102 (2002).
7. P. J. Feibelman, Science. **295**, 99 (2002).
8. J. Weissenrieder, A. Mikkelsen, J. N. Andersen, P. J. Feibelman, and G. Held, Phys. Rev. Lett. **93**, 196102 (2004).
9. K. Andersson, A. Nikitin, L. G. M. Pettersson, A. Nilsson, and H. Ogasawara, Phys. Rev. Lett. **93**, 196101 (2004).
10. N. S. Faradzhev, K. L. Kostov, P. Feulner, T. E. Madey, and D. Menzel, Chem. Phys. Lett. **415**, 165 (2005).
11. K. Andersson, A. Gómez, C. Glover, D. Nordlund, H. Öström, T. Schiros, O. Takahashi, H. Ogasawara, L. G. M. Pettersson, and A. Nilsson, Surf. Sci. **585**, L183 (2005).
12. C. Clay, S. Haq, and A. Hodgson, Chem. Phys. Lett. **388**, 89 (2004).
13. S. Haq, C. Clay, G. R. Darling, G. Zimbitas, and A. Hodgson, Phys. Rev. B. **73**, 115414 (2006).
14. D. N. Denzler, Ch. Hess, R. Dudek, S. Wagner, Ch. Frinchkorn, M. Wolf, and G. Ertl, Chem. Phys. Lett. **376**, 618 (2003).
15. G. Zimbitas, S. Haq, and A. Hodgson, J. Chem. Phys. **123**, 174701 (2005).
16. A. Glebov, A. P. Graham, A. Menzel, and J. P. Toennies, J. Chem. Phys. **106**, 9382 (1997).
17. S. Meng, E. G. Wang, and S. Gao, Phys. Rev. B. **69**, 195404 (2004).
18. M Morgenstern, J. Muller, T. Michely, and G. Comsa, Z. Phys. Chem. **198**, 43 (1997).
19. J. Cerdá, A. Michaelides, M. –L. Bocquet, P. J. Feiblman, T. Mitsui, M. Rose, E. Fomin, and M. Salmeron, Phys. Rev. Lett. **93**, 116101 (2004).
20. S. Meng, L. F. Xu, E. G. Wang, and S. Gao, Phys. Rev. Lett. **89**, 176104 (2002).
21. S. Meng, E. G. Wang, Ch. Frischkorn, M. Wolf, and S. Gao, Chem. Phys. Lett. **402**, 384 (2005).
22. A. Michaelides, A. Alavi, and D. A. King, Phys. Rev. B. **69**, 113404 (2004).
23. P. Vassilev, R. A. van Santen, and M. T. M. Koper, J. Chem. Phys. **122**, 054701 (2005).

24. G. A. Kimmel, N. G. Petric, Z. Dohnálek, and B. D. Kay, Phys. Rev. Lett. **95**, 166102 (2005).
25. G. A. Kimmel, N. G. Petric, Z. Dohnálek, and B. D. Kay, J. Chem. Phys. **126**, 114702 (2007).
26. S. Haq and A. Hodgson, J. Phys. Chem. C. **111**, 5946 (2007).
27. T. Kondo, H.S. Kato, M. Bonn, and M. Kawai, J. Chem. Phy. **126**, 181103 (2007).
28. M. E. Gallagher, S. Haq, A. Omer, and A. Hodgson, Surf. Sci. **601**, 268 (2007).
29. J. J. Zinck and W. H. Weinberg, J. Vac. Sci. Technol. **17**, 188 (1980).
30. J. Kiss and F. Solymosi, Surf. Sci. **177**, 191 (1986).
31. F. T. Wagner and T. E. Moylan, Surf. Sci. **191**, 121 (1987).
32. K. D. Gibson, M. Viste, and S. J. Sibener, J. Chem. Phys. **112**, 9582 (2000).
33. S. Yamamoto, A. Beniya, K. Mukai, Y. Yamashita, and J. Yoshinobu, J. Phys. Chem. B. **109**, 5816 (2005).
34. P. J. Feibelman, Phy. Rev. Lett. **90**, 186103 (2003).
35. S. Semancik, G. L. Haller, and J. T. Yates, Jr., Appl. Surf. Sci. **10**, 546 (1982).
36. R. Linke, D. Curulla, M. J. P. Hopstaken, and J. W. Niemantsverdriet, J. Chem. Phys. **115**, 8209 (2001).
37. M. A. Van Hove, W. H. Weinberg, and C. –M. Chan, *Low-Energy Electron Diffraction* (Springer, Berlin, Heidelberg 1986).
38. J. Yoshinobu and M. Kawai, Surf. Sci. **368**, 247 (1996).
39. V. Buch and J. P. Devlin, J. Chem. Phys. **94**, 4091 (1991).
40. J. P. Devlin, J. Geophys. Res. **106(E12)**, 33333 (2001).
41. H. Ogasawara, J. Yoshinobu, and M. Kawai, Chem. Phys. Lett. **231**, 188 (1994).
42. H. Ibach and S. Lehwald, Surf. Sci. **91**, 187 (1980).
43. B. Rowland and J. P. Devlin, J. Chem. Phys. **94**, 812 (1991).
44. M. W. Severson, J. P. Devlin, and V. Buch, J. Chem. Phys. **119**, 4449 (2003).
45. T. Yamada, H. Okuyama, T. Aruga, and M. Nishijima, J. Phys. Chem. B. **107**, 13962 (2003).
46. F. T. Wagner and T. E. Moylan, Surf. Sci. **182**, 125 (1987).
47. J. P. Devlin and V. Buch, J. Phys. Chem. **99**, 16534 (1995).
48. G. A. Kimmel, Z. Dohnálek, K. P. Stevenson, R. S. Smith, and B. D. Kay, J. Chem. Phys. **114**, 5295 (2001).
49. P. J. Feibelman and A. Alavi, J. Phys. Chem. B. **108**, 14362 (2004).
50. S. M. Dounce, S–H. Jen, M. Yang, and H–L. Dai, J. Chem. Phys. **122**, 204703 (2005).
51. P. J. Feibelman, Phys. Rev. B. **72**, 113405 (2005).
52. X. Su, L. Lianos, Y. R. Shen, and G. A. Somorjai, Phy. Rev. Lett. **80**, 1533 (1998).
53. B. J. Hinch and L. H. Dubois, Surf. Sci. **181**, 10 (1991).
54. M. Yang and H-L. Dai, J. Chem. Phys. **118**, 5106 (2003).
55. B. D. Kay, K. R. Lykke, J. R. Creighton, and S. J. Ward, J. Chem. Phys. **91**, 5120 (1989).

Chapter 8

Concluding remarks

In this study, the adsorption, desorption, and thin film growth of water molecules on Rh(111) were investigated. An Rh(111) surface is one of the few substrates where lattice mismatch with the basal plane of I_h is very small, and has not been studies so much as compared with other substrate such as Pt(111) and Ru(0001). Much previous literature on the adsorbed water on metal surfaces may have been affected by x-ray and/or electron induced modification, thus non- or less destructive experimental methods were used including IRAS, SPA-LEED, and TPD. In addition, surface impurities and defects were carefully controlled. The main topics of the present work are to clarify the following points: (1) transient diffusion and cluster formation of water molecules at low temperature. (2) the adsorption and desorption kinetics. (3) the first layer and thin film growth.

In Chapter 5, the initial stage of water adsorption on Rh(111) at 20 K was investigated. In this low coverage region, isolated water molecules and small water clusters are observed. Since thermal diffusion is suppressed at 20 K, the formation of water clusters at low coverage is controlled by both coverage and transient diffusion on the surface. Within a simple isotropic diffusion model as the transient diffusion and clustering process, I estimate the mean lateral

displacement from the first impact point to the final adsorption site to be 7.6 Å; an incoming water molecule on Rh(111) is trapped with eight post-collision hops on the average.

In Chapter 6, the adsorption and desorption kinetics of water molecules on the Rh(111) surface were investigated using temperature programed desorption. Water molecules show a coverage dependent sticking probability and initial sticking probability was estimated to be 0.46. Prior to desorption, water molecules exhibit coexistence of a dilute, gas like phase together with islands of a condensed phase, both being two dimensional. Apparent fractional-order desorption can be interpreted as a desorption from two-phase adsorbate with different sticking probabilities. And then, coverage dependence of activation energy and preexponential factor for desorption were estimated. As a result it is clarified that the first layer is energetically stable compared with the multilayer film, and this is clear evidence of wetting.

In Chapter 7, the adsorption states and growth process of the first water (D_2O) layer and multilayer on Rh(111) were investigated. At the initial stage, water molecules form the commensurate ($\sqrt{3}x\sqrt{3}$)*R*30°structure. This is flatter than the ice-like bilayer, and consists of the D-down species. D-down islands may have jagged circumference or anisotropic island shape. With increasing coverage, ice-like bilayer (D-up) grows and show a incommensurate structure. At nearly the saturation coverage, the ice-like bilayer is ~9 % compressed from the commensurate ($\sqrt{3}x\sqrt{3}$)*R*30°structure, which is ~5% compression with respect to ice I_h. At saturation coverage, the first water layer consists of the ice-like bilayer (D-up) and flat (D-down) domains, where the D-up domains occupy 44 % and the D-down domains occupy 56 % in coverage. Further adsorption of water molecules form 3D ice crystallites on the D-down domains where the D-down species do not reorient to accommodate formation of a crystalline ice. This is clear evidence of the hydrophobic first water layer.

In concluding, this thesis set out to understand the microscopic behavior

and structure of water on the Rh(111) surface using modern surface science techniques. The present study is the first time to reveal the limited transient diffusion length of water molecules because of large corrugated PES. This could be important to understand surface reactions including water molecules, because the adsorption dynamics could controls the reaction kinetics. In this study, energetical stabilization of the first water layer relative to the multilayer formation is elucidated, which is clear evidence of the molecular wetting layer. In addition, its structure is revealed. It shows the coverage dependent structures, where they significantly affect the growth mechanism of crystalline ice. The results in this thesis will improve our understanding of water-metal interactions being important in many scientific fields.

List of Figures

List of Tables

List of Publications

Papers included in this thesis:

1. "Transient diffusion and cluster formation of water molecules on Rh(111) at 20 K",
   A. Beniya, K. Mukai, Y. Yamashita, and J. Yoshinobu: J. Chem. Phys. **126**, 141102 (2007).
2. "The first water layer on Rh(111): Microscopic structure and desorption kinetics"
   A. Beniya, S. Yamamoto, K. Mukai, Y. Yamashita, and J. Yoshinobu:
   J. Chem. Phys.**125**, 054717 (2006).
3. "The first layer and crystalline ice growth of water molecules on Rh(111)"
   A. Beniya, K. Mukai, Y. Yamashita, and J. Yoshinobu: in preparation.
4. "Adsorption and desorption kinetics of water molecules on Rh(111)"
   A. Beniya, K. Mukai, Y. Yamashita, and J. Yoshinobu: in preparation.

Papers to which I have contributed but which are not included in this thesis:

1. "Water adsorption on Rh(111) at 20 K: from monomer to bulk amorphous ice"
   S. Yamamoto, A. Beniya, K. Mukai, Y. Yamashita, and J. Yoshinobu:
   J. Phys. Chem. B, **109**, 5816 (2005).
2. "Low Energy Electron Stimulated Chemical Reactions of CO in Water Ice"
   S. Yamamoto, A. Beniya, K. Mukai, Y. Yamashita, and J. Yoshinobu:
   Chem. Phys. Lett, **388**, 384 (2004).

Adsorption, desorption and thin film growth of water molecules on the Rh(111) surface

December, 2007

Atsushi Beniya